Master's Thesis
석사 학위논문

Investigations on Interfacial Reactions of Electrolytes on Carboneous and Magnesium Anodes for Rechargeable Lithium and Magnesium Batteries

Sungjin Kang(강 성 진 姜 成 振)

Department of Energy Systems Engineering
에너지시스템공학 전공

DGIST

2014

Master's Thesis
석사 학위논문

Investigations on Interfacial Reactions of Electrolytes on Carboneous and Magnesium Anodes for Rechargeable Lithium and Magnesium Batteries

Sungjin Kang(강 성 진 姜 成 振)

Department of Energy Systems Engineering
에너지시스템공학 전공

DGIST

2014

Investigations on Interfacial Reactions of Electrolytes on Carboneous and

Magnesium Anodes for Rechargeable Lithium and Magnesium Batteries

Advisor   :   Professor 이호춘

Co-advisor :   Doctor 김재현

by

강성진

Department of Energy Systems Engineering
DGIST

A thesis submitted to the faculty of DGIST in partial fulfillment of the requirements for the degree of Master of Science in the Department of Energy Systems Engineering. The study was conducted in accordance with Code of Research Ethics[1]

11. 15. 2013

Approved by

Professor 이 호 춘 _____ (Signature)
(Advisor)

Doctor 김 재 현 _____ (Signature)
(Co-Advisor)

---

[1] Declaration of Ethical Conduct in Research: I, as a graduate student of DGIST, hereby declare that I have not committed any acts that may damage the credibility of my research. These include, but are not limited to: falsification, thesis written by someone else, distortion of research findings or plagiarism. I affirm that my thesis contains honest conclusions based on my own careful research under the guidance of my thesis advisor.

Investigations on Interfacial Reactions of Electrolytes on Carboneous and Magnesium Anodes for Rechargeable Lithium and Magnesium Batteries

강 성 진

Accepted in partial fulfillment of the requirements for the degree of Master of Science.

11. 15. 2013

Head of Committee _____(인)
Prof. 이호춘

Committee Member _____(인)
Dr. 김재현

Committee Member _____(인)
Prof. 홍승태

ABSTRACT

This study investigated the effects of HF, an impurity in $LiPF_6$ electrolytes, on redox reactions of graphite anodes for the lithium-ion batteries (LIBs) and electrolyte solution for magnesium-ion batteries were developed, based on sulfone group solution, non-Grignard reagents.

In the first place, it is found that pyrolytic graphite edge plane electrode (PGE) presents reversible Li^+ transport behavior in $LiClO_4$ solution, but suppressed intercalation/de-intercalation reaction in $LiPF_6$ electrolyte. The sluggish intercalation/de-intercalation reaction in $LiPF_6$ is progressed by adding a HF scavenger, whereas the facile intercalation/de-intercalation reaction in $LiClO_4$ is depressed by adding HF. In addition, the Li^+ transport in $LiPF_6$ is enhanced by decreasing electrolyte volume or by increasing PGE surface area. These behaviors are attributed to the HF-induced formation of LiF layer on graphite anode surface, which is facilitated at high ratio of electrolyte volume to electrode area (V/A ratio). The electrolyte-volume-to-electrode-area ratio affects the Li^+ transport behavior of the graphite composite electrodes for commercial grade LIBs. This study explains on an age-old question: why Li^+ transport behavior of graphite anode in $LiPF_6$ is suppressed in flooded cells, but not in commercial LIBs. Areas of electrode surface were carried out by double-layer capacitances (C_{dl}) which related to a fraction of edge (f_e).

Lastly, it is necessary that new electrolyte of reversible magnesium system is developed instead of Grignard-based because of its unstable chemically and electrochemically. Sulfone-based solutions are one of good candidates. Dialkyl sulfones ($R_1R_2SO_2$) such as dipropyl sulfone ($DPSO_2$), ethyl-methyl sulfone ($EMSO_2$) and dibutyl sulfone ($DBSO_2$) were performed with conventional magnesium salt ($MgCl_2$) in CVs. Eutectic of sulfone-based electrolyte and co-solvent with sulfone electrolyte were performed. Especially, cell performances were enhanced when adding tetrahydrofuran (THF) in dialkyl sulfone electrolyte by volume ration one to one (1/1 = v/v). The high performance sulfone electrolyte such as DPSO2 and DPSO2/THF were compared with their characteristics such as ionic conductivity. Ionic conductivity is improved with adding THF in sulfone solution. Besides the study of cathode materials and current collectors, incompatibility between the electrolytes, which may be related to the chemical instability of the Grignard reagent-based electrolyte, is also critical issues for rechargeable Mg battery with a good performance. Therefore, understanding the electrochemical behavior of current collectors and synthesis of stable electrolyte are critical for Mg batteries.

Keywords: Li-ion batteries, HF, LiF, Mg-ion batteries, Sulfone electrolyte

Contents

Tables

Table 1. Atomic percentages derived from XPS measurements in Fig. 10.

Table 2. Double-layer capacitance (C_{dl}) and fraction of edge (f_e) of emery-PGE and alumina-PGE.

Table 3. Practical capacities and efficiencies of thin and thick electrodes during CVs from Fig. 9 (scan rate: 5 mVs^{-1}).

Table 4. Practical capacities and efficiencies of thin and thick electrodes during CVs from Fig. 10 (scan rate: 0.5 mVs^{-1}).

Table 5. Deposition / dissolution efficiency of Mg bis(diisopropyl) amide solution (0.7M THF) electrolyte on Mg and Pt electrodes.

Table 6. Melting points of sulfones.

Table 7. Efficiencies of singular sulfone-based electrolyte.

Table 8. Efficiencies of sulfone-based eutectic electrolyte.

Table 9. Efficiencies of EMSO$_2$, DPSO$_2$ and DBSO$_2$ with THF (1/1, vol) electrolyte.

Table 10. Efficiency of DPSO$_2$/THF dependant on volume ratio (v/v) on Pt and Edge electrodes at 30 ^{o}C and 60 ^{o}C.

Table 11. Efficiency of DPSO$_2$ alone and DPSO$_2$/THF (1/1, v/v) on Pt and Edge electrodes.

Figures

Fig. 1. (Left) Edge and Basal planes of graphite, (Right) commercial edge plane graphite electrode used in this study.

Fig. 2. Scheme of (Left) rechargeable system in Li battery, (Right) not possible in Mg battery with conventional electrolyte system.

Fig. 3. Scheme of cathode is corroded by Grignard reagent-based electrolyte.

Fig. 4. Scheme of pretreatment of Mg plate for counter / reference and stacking components of 2032 2-electrode coin cell

Fig. 5. CVs of emery-PGEs in EC/DEC (1/2, v/v) solutions of (a) 1 M $LiClO_4$ and (b) 1 M $LiPF_6$.

Fig. 6. CVs of emery-PGEs in EC/DEC (1/2, v/v) solutions of (a) 1 M $LiClO_4$ + 100 ppm HF and (b) 1 M $LiPF_6$ + 5 wt % HMDS.

Fig. 7. CVs of alumina-PGEs in EC/DEC (1/2, v/v) solutions of (a) 1 M LiClO4 and (b) 1 M LiPF6.

Fig. 8. CV of emery-PGE in 1 M $LiPF_6$ EC/DEC (1/2, v/v) solution. The amount of electrolyte was reduced to 0.04 mL from 4 mL. Two electrode configuration was employed.

Fig. 9. CVs of (a) thin (2.1 mg/cm^2) and (b) thin (9.4 mg/cm^2) graphite composite electrodes in 1 M $LiPF_6$ EC/DEC (1/2, v/v) solution.

Fig. 10. XPS spectra for the graphite composite electrodes subjected to ten CV cycles over 0.2–3.5 V in 1 M $LiPF_6$ EC/DEC (1/2, v/v) solution. (a) thin and (b) thick graphite composite electrodes.

Fig. 11. CVs of (a) emery paper polished PGE, (b) alumina polished PGE in 1M KCl, scan rate from 500 m Vs^{-1} to 5,000 mVs^{-1} within the potential range of -5 mV to 5 mV (vs. Ag/AgCl). (c) Slopes of the steady-state current versus scan rate: emery paper (■), alumina (▲).

Fig. 12. Schematic diagram of the Li^+ ion transport of graphite anode in a $LiPF_6$ solution. (a) the V/A ratio is high, and thus the Li^+ ion transport is suppressed. The ratio is low (b) due to increased electrode area, and (c) due to decreased electrolyte volume, enabling facile Li^+ ion transport.

Fig. 13. CVs of (a) thin (0.15 mAh) and (b) thick (0.54 mAh) graphite composite electrodes in 1 M $LiPF_6$ EC/DEC (1/2, v/v) solution at scan rate 0.5 mVs^{-1}.

Fig. 14. CVs of (a) Mg working and (b) Pt working electrode in Mg bis(diisopropyl) amide solution (0.7 M THF) electrolyte at scan rate 20 mVs^{-1} and structure of Mg bis(diisopropyl) amide solution (inset).

Fig. 15. Cyclic voltammogram showing magnesium deposition/dissolution on (a) Pt electrode, 45 ^{o}C (b) GC, 45 ^{o}C (c) Pt, 65 ^{o}C and (d) GC, 65 ^{o}C in 2M $MgCl_2$/$EMSO_2$ electrolyte at a voltage scan rate of 10mVs^{-1} within the potential range of -1 to 3.1 V (vs. Mg/Mg^{2+})

Fig. 16. CV of 1M $MgCl_2$/$DPSO_2$ electrolyte on (a) Pt electrode, 35 ^{o}C (b) PGE, 35 ^{o}C (c) Pt, 60 ^{o}C and (d) PGE, 60 ^{o}C in at a voltage scan rate of 20mVs^{-1} within the potential range of -1.5 to 3.3 V (vs. Mg/Mg^{2+})

Fig. 17. CV of 1M $MgCl_2$ / $DBSO_2$ electrolyte on (a) Pt electrode, 60 ^{o}C and (b) PGE, 60 ^{o}C in at a voltage scan rate of 20mVs^{-1} within the potential range of -1.5 to 3 V (vs. Mg/Mg^{2+}). (c) After CV experiment in 3-electrode configuration, electrolyte was solidified (red arrow).

Fig. 18. CV of $MgCl_2$ / $EMSO_2$ / $DMSO_2$ (0.35/3/1, wt %) eutectic electrolyte on (a) Pt electrode, 35 ^{o}C (b) PGE, 35 ^{o}C (c) Pt, 60 ^{o}C and (d) PGE, 60 ^{o}C in at a voltage scan rate of 20mVs^{-1} within the potential range of -1.5 to 3.3 V and 3.5 V (vs. Mg/Mg^{2+}).

Fig. 19. CV of 1M $MgCl_2$ / $EMSO_2$ + $DBSO_2$ (1/1, vol %) eutectic electrolyte on (a) Pt electrode, 35 ^{o}C (b) PGE, 35 ^{o}C (c) Pt, 60 ^{o}C and (d) PGE, 60 ^{o}C in at a voltage scan rate of 20mVs^{-1} within the potential range of -1.5 to 3.3 V and 3.5 V (vs. Mg/Mg^{2+}).

Fig. 20. CV of 1M $MgCl_2$ / $DPSO_2$ + $DBSO_2$ (1/1, vol %) electrolyte on (a) Pt electrode, 60 ^{o}C and (b) PGE, 60 ^{o}C in at a voltage scan rate of 20mVs^{-1} within the potential range of -1.5 to 3 V (vs. Mg/Mg^{2+}).

Fig. 21. CV of sulfones with THF (1/1, vol) electrolyte containing 0.8M $MgCl_2$. (a) $EMSO_2$/THF on Pt electrode, (b) $EMSO_2$/THF on PGE, (c) $DPSO_2$/THF on Pt, (d) $DPSO_2$/THF on PGE, (e) $DBSO_2$/THF on Pt, and (f) $DBSO_2$/THF on PGE in at a voltage scan rate of 20mVs^{-1} within the potential range of -1.5 to 3.3 V (vs. Mg/Mg^{2+}) at 30 ^{o}C

Ⅰ. INTRODUCTION

1.1 Li-ion battery: Suppressive effects of electrolyte-volume-to-electrode-area ratio (V/A ratio) on redox behaviors of graphite anodes

To date, the most studies on the graphite anode have been carried out using the graphite composite electrode. In contrast to the standardized novel electrodes (Pt, Au, Glassy carbon), however, the graphite composite electrode has several intrinsic limitations in its usage: First, the composite electrode is not reusable: proper refreshing method for porous composite electrodes is, if any, not available at present. Second, the reproducible fabrication of the composite electrodes is challenging: the electrode design parameters (thickness, density, porosity, and loading level), which greatly affect the electrochemical responses of the electrode, have to be precisely controlled. Third, the composite electrodes are subject to the interference from the other ingredients: polymeric binder and conductive carbon. Forth, it is almost impossible to investigate separately the electrochemical reactions of the edge and basal planes

As an alternative to the composite electrode, a novel electrode has long been used for the examination on the cathodic reactions of the electrolyte, but its implication is very limited due to the inherent difference between the two. Considering the material similarity, the highly ordered pyrolytic graphite (HOPG) electrodes are much preferred to the novel metal electrode. Moreover, one of the edge and basal planes of HOPG can be preferentially exposed, thus enabling the examination of the individual performances of the edge or basal plane. HOPG electrodes have been employed so far to give valuable information relevant to the graphite anode performances such as SEI formation/degradation and Li^+ ion transport kinetics. [1−4] However, the electrochemical aspects of the edge and basal planes of graphite anode are yet fully understood. Also, the most of previous HOPG experiments were performed in $LiClO_4$ solutions, rather not in $LiPF_6$ solutions that are more important in practical applications.

In this study, it was revealed that the cyclic voltammograms (CVs) of pyrolytic graphite edge plane electrode (PGE) in a LiPF$_6$ solution are dramatically different from those in LiClO$_4$ solution. The reversible Li$^+$ intercalation/de-intercalation reaction is observed in LiClO$_4$ solution, whereas the redox reaction is severely suppresses in LiPF$_6$ solution. In addition, the redox behaviors of PGEs greatly depend on the surface area. The emery-PGEs, supposed to have much larger surface area, showed much enhanced redox activities compared with the alumina-PGE. We suggested that the HF impurity, an inevitably impurity present in a LiPF$_6$, induces LiF-abundant SEI, which is responsible for the severe passivation, and thus the suppressed Li$^+$ transport kinetics in a LiPF$_6$ solutions. More importantly, the ratio of the electrolyte volume to the electrode surface (hereafter the V/A ratio) was claimed to be responsible for the different CVs of the alumina/emery-PGEs. Our results clearly demonstrate that HF impurity suppresses the Li$^+$ transport kinetics of graphite anode and that the extent of HF influence is determined by the V/A ratio. Comparison of electrodes area was measured by double-layer capacitances (C_{dl}) of emery-PGE and alumina-PGE because active site of graphite electrode depends on the fraction of edge (f_e) which related to C_{dl}. Furthermore, practical and theoretical capacities were calculated in this study.
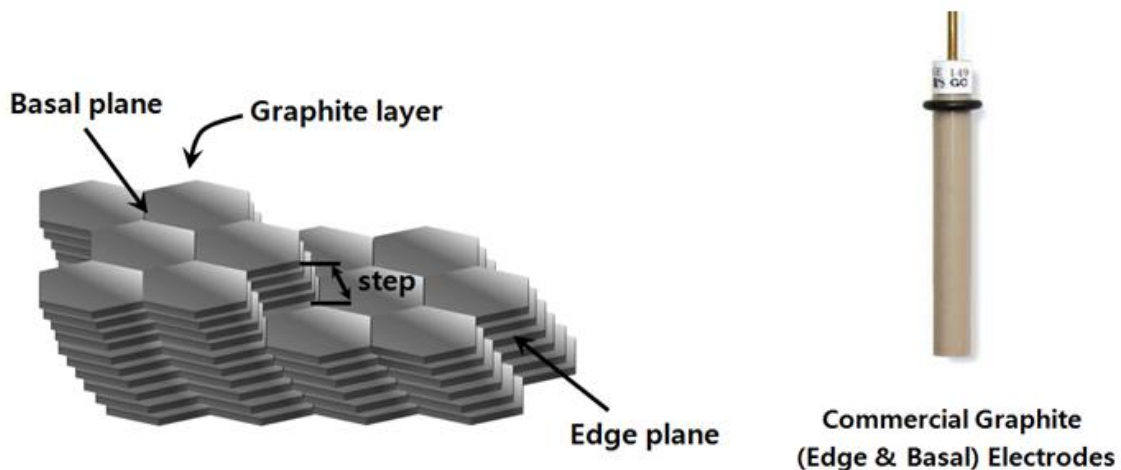
Fig. 1. (Left) Edge and Basal planes of graphite, (Right) commercial edge plane graphite electrode used in this study.

1.2 Mg-ion battery: Sulfone electrolytes for rechargeable magnesium system

Electrical vehicles (EVs) which use secondary batteries have attracted world-wide attention demanding environmental issues in recent years. The secondary battery has critical role in EVs. Especially energy density, performance and cost are the major issues in the successful application for this kind of transportation. Lithium-ion batteries are the most usages for EVs but it cannot satisfy all the requirements such as low cost, high energy and power density, high safety, etc. Therefore, development of post-lithium battery which is green and safer, cheaper is critical. Recently, rechargeable Mg batteries is recognized as promising storage applications for next-generation rechargeable batteries since Mg has very negative electrode potential (-2.37 V vs. SHE) and high theoretical specific capacity of 3830 mAh/cm^3. Especially, Mg is environmentally benign, safety, abundance in the earth's crust ($\sim$13.9% Mg compared to $\sim$0.0007% of Li) and low raw material cost(($\sim$\$ 2700/ton for Mg compared to \$64,000/ton for Li) compared to lithium. Furthermore, since the magnesium ion has the bivalent nature (Mg^{2+}), a suitable intercalation anode and cathode if identified could generate twice the capacity of the best intercalation hosts available for Li-ion (single valent Li$^+$) batteries. Therefore, for post lithium ion battery candidate magnesium (Mg) is very promising material above reasons. [5-10] However, in comparison with the development of rechargeable Li batteries, rechargeable Mg battery system is still at the beginning stage. In contrast to Li batteries, there are several serious challenges for the development of practical Mg based batteries, such as lack of proper cathode materials, limited selectivity of practical electrolyte systems with reversible Mg deposition and a narrow electrochemical window.

One of the biggest challenges in developing rechargeable Mg batteries system is to find a suitable electrolyte. While Li batteries use electrolytes containing conventional Li salt such as, LiPF$_6$ and LiClO$_4$, dissolved in organic carbonate-based solvents, such as mixtures of ethylene carbonate (EC), diethyl carbonate (DEC) or propylene carbonate (PC), practical analogs of these electrolytes for Mg-based batteries have not been demonstrated. Mg salts (perchlorate, chloride, triflate) have low solubility in such solvents. [11, 12]

The reason why those electrolytes were not demonstrated with Mg salt is because of critical barrier as like forming a Mg^{2+} blocking layer on the surfaces of electrodes using conventional battery electrolytes during driven cell. (Fig. 2)
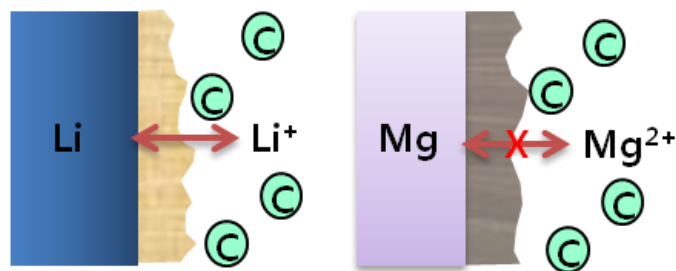
Fig. 2. Scheme of (Left) rechargeable system in Li battery, (Right) not possible in Mg battery with conventional electrolyte system.

In spite of those limitations, electrochemically reversible magnesium deposition/ dissolution batteries were first demonstrated by Aurbach et al.[10, 13-18] It is well known that Mg electrodes display highly reversible behavior in organometallic Mg salt solutions such as Grignard salts, amidomagnesium halides, or magnesium organoborates (RMgX, R=alkyl, aryl groups; X=Cl, Br) in ether solutions. [19-20] Magnesium battery electrolyte of Grignard reagents overcomes the low anionic stability. However, the main problem of this magnesium organohaloaluminate electrolyte was the electrochemical instability. [21] The electrochemical stability window was improved by substituting alkyl groups on the Lewis acid with phenyl groups. Therefore, organohaloaluminate called APC formed from the reaction of one equivalent of $AlCl_3$ with two equivalents of PhMgCl displayed a much improved electrochemically stable window of 3.3V vs. Mg. Unfortunately, the in situ generated magnesium organohaloaluminates reported so far, while having high columbic efficiencies, are nucleophilic, and air sensitive. Grignard reagent-based electrolytes are very unstable chemically and electrochemically. [22, 23] The chemical instability of the Grignard reagent-based electrolyte could lead to electrochemical incompatibility with the other components of the battery system,

including the cathode, anode, separator, and current collectors. It is well known that compatibility between current collectors and electrolyte, particularly the stability of current collectors, is an important factor for designing a rechargeable battery with a long cycle life. Recently, stability of cathodes such as Chevrel phase (Mo_6S_8) which are usually corrosive for non-noble metals is one of critical issues in Mg battery systems. Therefore, conducting a fundamental study and understanding the electrochemical behavior of current collectors in electrolyte for Mg-ion batteries is also critical for practical applications. At voltages higher than about 2.5 V vs. Mg, the electrolyte of Grignard reagents caused the corrosion of stainless steel onset voltage (Fig. 3). [24, 25] Therefore, it is necessary that affordable and stable electrolytes should be explored as Mg rechargeable batteries using conventional magnesium salt.
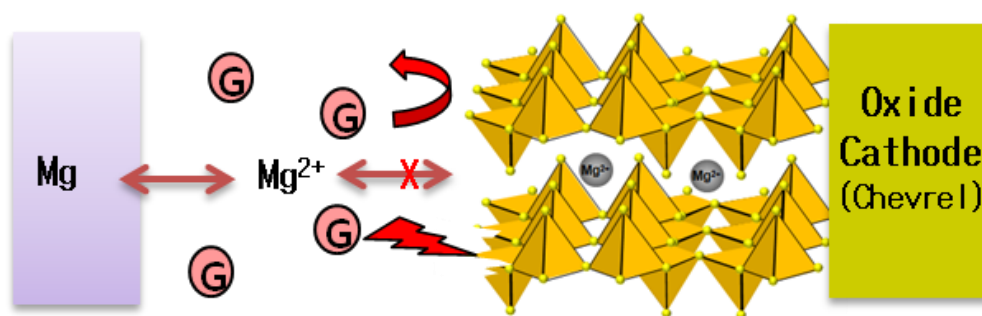
Fig. 3. Scheme of cathode is corroded by Grignard reagent-based electrolyte.

Here we present a detailed study of sulfone-based reagents which were chosen as candidate host solvent for electrolyte for Mg-based batteries. Because sulfone-based reagents are stable in simple atmosphere not like Grignard reagent, it has wider electrochemical stability (over about 3.1V vs. Mg). In addition, sulfone-based electrolyte is able to dissolve magnesium chloride ($MgCl_2$), conventional magnesium salt. Dipropyl sulfone (DPSO2) / tetrahydrofuran (THF) (1/1, vol) solvent performed high deposition and dissolution efficiency (over 80%). Remarkably, it was found that reversible Mg intercalation in Mo_6S_8 could be carried out in this electrolyte.

Furthermore, in this study, electrochemical behavior of current collectors in electrolyte for Mg-ion batteries is handled. Topic of current collectors has received little attention. Hence, in this study, the electrochemical stability of potential current collectors for Mg-ion batteries, such as platinum, nickel, stainless steel (SUS 304), and aluminum has been investigated in DPSO$_2$/THF electrolyte. Our results indicate that nickel is a good candidate as cathode and/or anode current collectors for Mg batteries in the present electrolyte due to its excellent electrochemical stability up to ～2.8 V. This is higher than the reported corrosion of Mg electrolyte for Grignard reagent.

Ⅱ. EXPERIMENTAL

2.1 Li-ion battery

2.1.1 Chemicals

$LiClO_4$ (99.99 %), HF (48 wt% in water), and hexamethyl disiloxane (HMDS) were purchased from Aldrich. Battery grade 1 M $LiPF_6$ ethylene carbonate (EC) / diethyl carbonate (DEC) (1/2, v/v) solution were provided by LG Chem.

2.1.2 Electrochemical measurements

A standard three-electrode configuration was employed, otherwise mentioned. Li and Pt wire were served as reference and counter electrodes, respectively. Pyrolytic graphite edge plane electrode (PGE, area = 0.70 cm^2) from ALS (Japan) was used as a working electrode. PGE was polished on emery paper (#3000, 7 μm grit size) or with alumina (0.3 μm diameter) slurry on a polishing pad. Hereafter, they are called emery-PGE and alumina-PGE, respectively. Cyclic voltammogram (CV) was performed at scan rate of 5 mV/s. The base electrolyte was a 1 M $LiClO_4$ or 1 M $LiPF_6$ in EC/DEC (1/2, v/v). The CV experiment in a flooded cell was performed with 4 mL of the electrolyte. For the CV experiment with small electrolyte amount, a two-electrode configuration was employed. A Li disk (14 mm diameter), serving as reference and counter electrodes, was covered with a PE separator (20 μm thick) soak with 0.04 mL electrolyte, on top of which PGE working electrode was placed gently to touch the separator.

Surface area was determined from the double-layer capacitance C_{dl}, which has been shown to increase with an increasing ratio of edge to basal planes. For measuring a fraction of edge plane, f_e of each condition (alumina polishing, emery paper polishing) was followed a paper from Newman group. [26] f_e is here defined as the fraction of total electrode area that exposes the edge plane to the electrolyte. f_b, the fraction of total electrode area that exposes the basal plane to the electrolyte, is equal to $1 - f_e$. Cyclic voltammograms were measured in 1.0M KCl with a Ag/AgCl reference and platinum counter electrode,

and C_{dl} was calculated from the variation of average current with scan rate. The potential limits were ±50 mV from the open-circuit potential, and the scan rate ranged from 500 to 5000 mV/s.

Graphite composite electrode was fabricated with artificial graphite with 3 wt% SBR and 2 wt% CMC on Cu foil (20 μm thick), with two different loading levels: 6.8 mg/cm^2 for a thicker electrode(10.5mg on Φ14mm Cu foil) and 1.9 mg/cm^2 for a thinner one(2.9mg on Φ14mm Cu foil). The coated composite electrode was cut into a piece with the same area as the PGE (0.07 cm^2), which was welded to a SUS strip wrapped with an insulation imide tape to be served as an electrical lead. All the electrochemical experiments were performed in an Ar-atmosphere glove box where H_2O and O_2 concentrations were kept below 5 ppm and temperature was held at 25±2 ℃.

X-ray photoelectron spectroscopy (XPS) measurements were performed in ESCALAB 250Xi (Thermo Scientific), with a monochromatic Al Kα source. For sample preparation, the graphite composite electrodes were subjected to ten CV cycles over 0.2 – 3.5 V in a flooded cell with 1 M $LiPF_6$ solution.

2.2 Mg-ion battery

2.2.1 Chemicals

Mg bis(diisopropyl) amide solution (0.7M THF) ($Mg[((CH_3)_2CH)_2N]_2$) were purchased from Aldrich. Ethyl methyl sulfone ($EMSO_2$), dipropyl sulfone ($DPSO_2$) and dimethyl sulfone ($DMSO_2$) were purchased from TCI Co. Tetrahydrofuran (THF) was purchased from Aldrich. Magnesium chloride ($MgCl_2$, ultra dry, 99.9%) were purchased from Alfa Aesar. All chemicals were used without further purification.

2.2.2 Electrochemical measurements

A lab-made three-electrode configuration was employed. Mg strips were served as reference and counter electrodes. Pyrolytic graphite edge plane electrode (PGE, area = 0.70 cm^2) and platinum disk electrode (Pt, Φ1.6mm, area = 0.02cm^2) from ALS (Japan) were used as a working electrode. PGE was polished on emery paper (#3000, 7 μm grit size) and Pt electrode was polished with alumina (0.3 μm diameter) slurry on a polishing pad. Mg strip electrodes were pretreated by polishing of emery-paper (#2,000). Cyclic

voltammogram (CV) was performed at scan rate of 20 mV/s. CV experiments were performed in an Ar-atmosphere glove box where H_2O and O_2 concentrations were kept below 5 ppm and temperature was held at 30±2 ℃. Ionic conductivity measurements were carried out ionic conductivity measure (Thermo Science) from 10 to 80 ℃.

Mo_6S_8 Chevrel phase electrode was fabricated with 80% artificial active mass, 10% PVDF binder, 10% carbon black on SUS foil (20 μm thick). This Chevrel phase electrode has 122 mAh/g theoretical capacity. The coated composite electrode was cut into a piece with 5 x 5 mm size, which was welded to a SUS strip for three-electrode configuration.

The 2-electrode coin cell stack (2032 type cell) consists of a conical spring, spacer, Chevrel or Pt working electrode, glass fiber separator, and Mg foil for a counter/reference electrode. Pretreatment of Mg plate for counter, reference electrode is shown schematically in Fig. 4. Mg plate was polished by knife mechanically, and then dipped in ethanol for 5min. It is stacked in coin cell for counter / reference electrode. All the pretreatment of Mg plate before producing coin cell was performed in an Ar-atmosphere glove box where H_2O and O_2 concentrations were kept below 5 ppm and temperature was held at 30±2 ℃. Coin cell tests were performed voltage limits which cut off voltage was set from -1 V to 1 V for Pt/Mg cell and from 0.3V to 1.8V for Mo_6S_8/Mg cell.
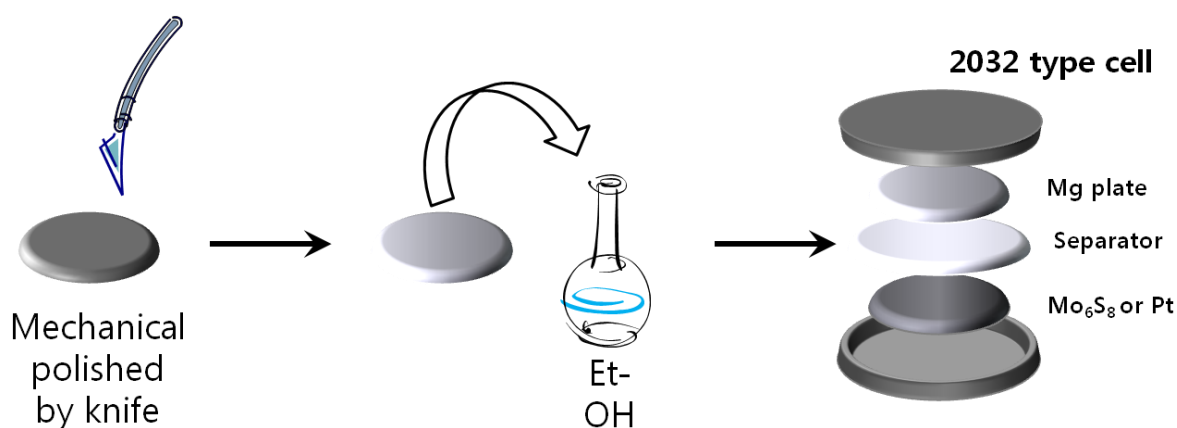
Fig. 4. Scheme of pretreatment of Mg plate for counter / reference and stacking components of 2032 2-electrode coin cell

Ⅲ. RESULTS AND DISCUSSION

3.1 Li-ion battery

3.1.1 Li salt effects on the Li$^+$ ion transport behavior of PGE: LiPF$_6$ vs. LiClO$_4$

The cyclic voltammograms (CVs) of emery polished PGE in 1 M LiClO$_4$ and 1 M LiPF$_6$ EC/DEC (1/2, v/v) electrolytes are compared in Fig. 5. Floored amount of electrolyte (4 mL) used for the CV measurements, which leads to the flooded cell condition. In LiClO$_4$ (Fig. 5a), the reduction current starts to flow below 1.0 V at the 1st cathodic sweep, and an oxidation peak is observed at 0.93 V at the following anodic sweep. The redox activity is maintained even after 10 consecutive cycles, which manifests the reversible nature of the Li$^+$ transport in LiClO$_4$. The reduction and oxidation currents are obviously assigned to the intercalation and the de-intercalation of Li$^+$ ion through PGE, respectively. The reduction current due to the solid electrolyte interphase (SEI) formation is not discernible at the 1st cathodic sweep. It seems that the SEI formation current is overlapped with much larger Li$^+$ intercalation response. Similar voltammetric behavior has also been reported previously for the edge plane of a mechanically polished HOPG in LiClO$_4$ solutions [1-3].

The CV in LiPF$_6$ (Fig. 5b) is quite different from that in LiClO$_4$ (Fig. 5a). It exhibits at the 1st cathodic sweep a distinct reduction peak at 0.49 V that keeps decreasing at the following cycles, which can be assigned to the SEI formation [4]. The reduction current tail after the reduction peak and the oxidation peak at 0.99 V at the following anodic scan can be traced to the Li$^+$ transport reaction as in the case of LiClO$_4$. The redox activity in LiPF$_6$ keeps decreasing with cycle and becomes negligible at the 10th cycle. In addition, the CV in LiPF$_6$ shows much smaller current scale at the 1st cycle than that in LiClO$_4$ (approximately by a factor of 2). These features points to sluggish Li$^+$ transport behavior in LiPF$_6$ in comparison with that in LiClO$_4$.
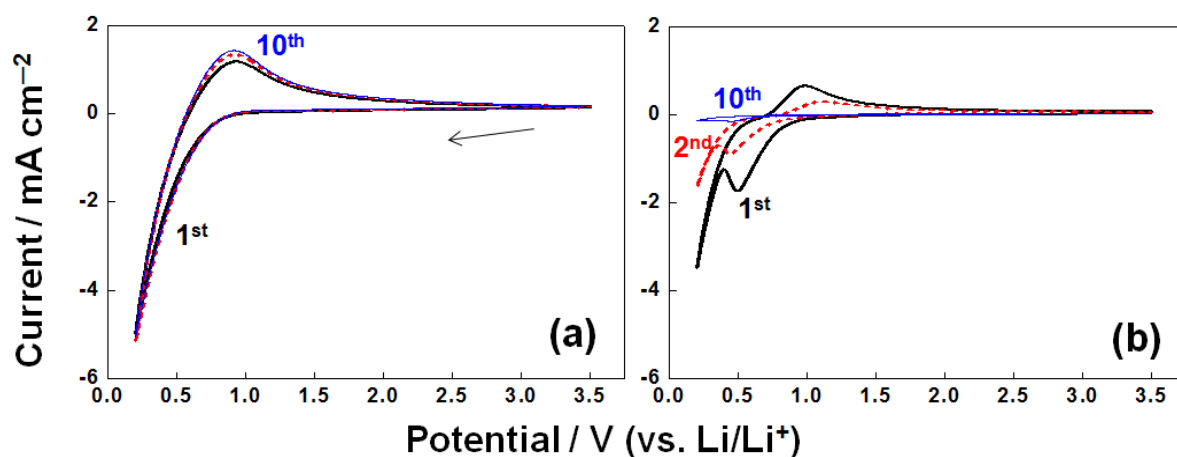
Fig. 5. CVs of emery-PGEs in EC/DEC (1/2, v/v) solutions of (a) 1 M LiClO$_4$ and (b) 1 M LiPF$_6$.

In order to reveal the origin of the different redox behavior of LiClO$_4$ and LiPF$_6$ solutions, the effects of HF, an inevitably impurity of LiPF$_6$ solution, was examined. The HF content of the LiPF$_6$ solution used in this study was determined to be about 60 ppm, and thus LiClO$_4$ solution was deliberately doped with 100 ppm HF (hereafter called LiClO$_4$+HF). Note that the CV in LiClO$_4$+HF (Fig. 6a) shows the same features as that in LiPF$_6$ (Fig. 5b): reduced current scale and decaying redox activity with cycle. As an alternative approach to check the influence of HF, 5 wt % hexamethyl disiloxane (HMDS), a HF scavenger [27], was added to LiPF$_6$ solution to remove HF present in LiPF$_6$ solution (hereafter called LiPF$_6$+HMDS). The 1st cycle CV of LiPF$_6$+HMDS (Fig. 6b) looks rather similar to that of LiPF$_6$ (Fig. 3b), but the redox activity in LiPF$_6$+HMDS is notably enhanced at the subsequent cycles to be comparable with that in LiClO$_4$. These results clearly indicate that the HF impurity is the key factor to suppress the Li$^+$ transport kinetics in LiPF$_6$ solution.
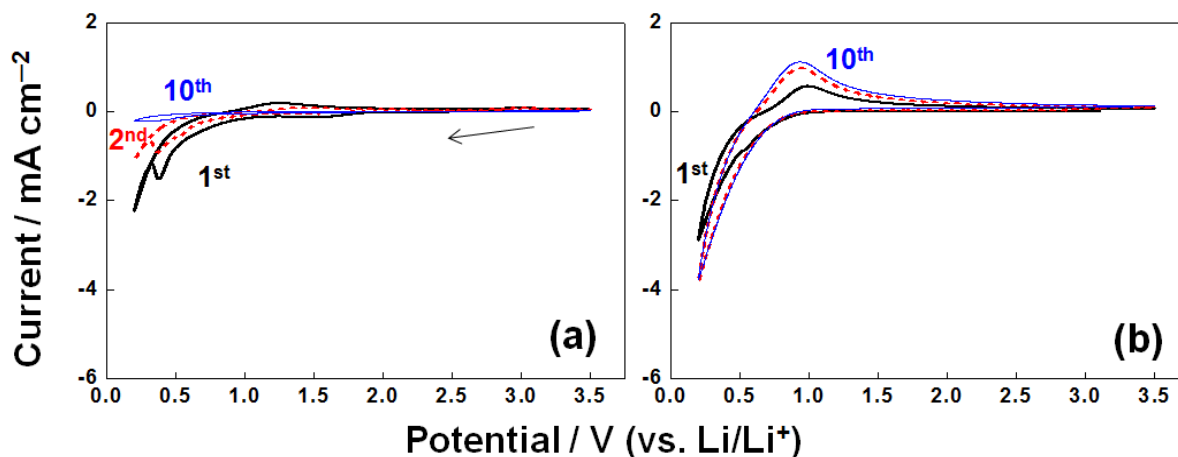
Fig. 6. CVs of emery-PGEs in EC/DEC (1/2, v/v) solutions of (a) 1 M LiClO$_4$ + 100 ppm HF and (b) 1 M LiPF$_6$ + 5 wt % HMDS.

3.1.2 Effects of the electrolyte-to-electrode area ratio (V/A ratio)

It has been claimed that the relative amount of electrolyte to the electrode surface area (V/A ratio) plays an important role in determining the surface chemistry of graphite anodes [28, 29]. In order to assess the impact of the V/A ratio, alumina slurry instead of emery paper was employed for PGE polishing to reduce the surface area of PGE (hereafter called alumina-PGE and emery-PGE). Considering finer grit size of the alumina (0.3 μm) than the emery paper (7 μm) used in this study, it is obvious that alumina-PGE possesses lower surface roughness and smaller surface area than emery-PGE, thus having larger the V/A ratio. As shown in Fig. 7a, the CV of alumina-PGE in LiClO$_4$ looks quite similar to that of emery-PGE (Fig. 5a), although the former shows somewhat decreased current at the 10th cycle. In stark contrast, the overall shape and the current scale of alumina-PGE in LiPF$_6$ (Fig. 7b) is significantly different from that of emery-PGE (Fig. 5b). After a reduction peak and a following current tail at the 1st cathodic scan, the CV of alumina-PGE in LiPF$_6$ (Fig. 7b) shows negligible oxidation current at the following anodic sweep, which points to the absence of Li$^+$ ion transport. In addition, the current becomes negligible from the 2nd cycle. Thus, it can be stated that the Li$^+$ transport of alumina-PGE is hindered more than that of emery-PGE, and that the hin-

drance is more severe in $LiPF_6$ than in $LiClO_4$. This indicates that the large V/A ratio is unfavorable to the Li^+ transport kinetics, especially in $LiPF_6$ solutions.
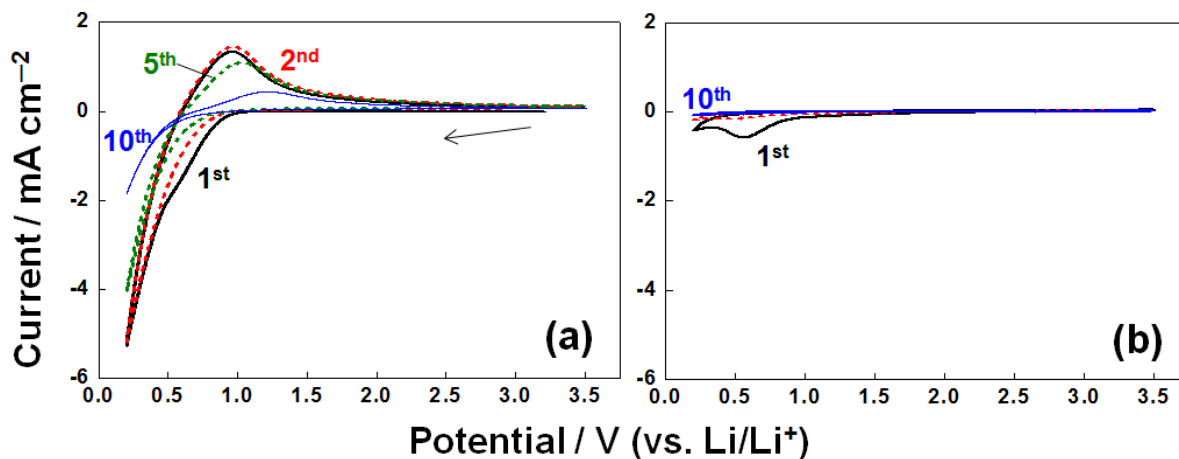
Fig. 7. CVs of alumina-PGEs in EC/DEC (1/2, v/v) solutions of (a) 1 M $LiClO_4$ and (b) 1 M $LiPF_6$.

For the crosscheck of the role of the V/A ratio, the CV of emery-PGE was obtained in a reduced volume (0.04 mL instead of 4 mL) of $LiPF_6$ solution to set the condition of the reduced V/A ratio. Note that the CV with 0.04 mL electrolyte (Fig. 8) exhibits much enhanced Li^+ transport kinetics compared with that with 4 mL electrolyte (Fig. 5b). It shows a similar CV response at the 1st cycle. But the current grows with cycle at the subsequent cycles and the current scale at the 10th cycle becomes comparable to those of HF-free cases ($LiClO_4$ in Fig. 5a and $LiPF_6$+HMDS in Fig. 6b). This clearly supports that the small V/A ratio is favorable to the Li^+ transport behavior in $LiPF_6$.
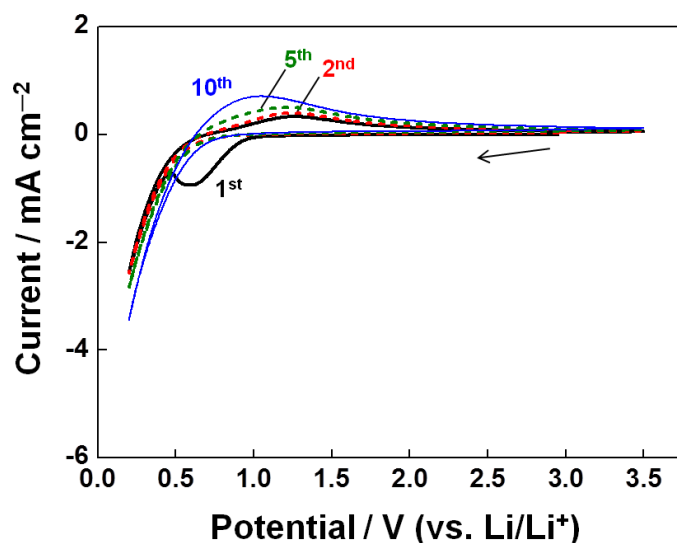
Fig. 8. CV of emery-PGE in 1 M LiPF$_6$ EC/DEC (1/2, v/v) solution. The amount of electrolyte was reduced to 0.04 mL from 4 mL. Two electrode configuration was employed.

The suppressive effect of HF on the Li$^+$ transport behavior of graphite electrode is rather unexpected since LiPF$_6$-based electrolytes are being commonly employed in current LIB industry. In order to address this issue, the impact of the V/A ratio on the CVs of the graphite composite electrode was investigated. The graphite composite electrodes were prepared with two different loading levels: the thinner electrode was prepared with a loading less than a quarter of the thicker electrode (2.1 and 9.4 mg/cm^2, respectively). It should be noted that the loading level of the thicker electrode prepared in this study corresponds approximately to the lower loading limit of commercial grade anodes. The tests of coin half cells (graphite composite/separator/Li), employing about 0.15 mL electrolyte, confirmed that both types of the composite electrodes exhibits decent cycle performances at least up to 50th cycle (not shown here). For the CV experiments with a three electrode configuration with 4 mL electrolyte, the thin electrode keeps losing its Li$^+$ transport activity with cycle, and it shows a featureless CV with only capacitive current at the 10th cycle (Fig. 9a). On the other hand, the thick electrode retains considerable activity even after the 10th cycle (Fig. 9b). This clear-

ly proves that the Li$^+$ transport behavior of graphite composite electrodes is also greatly affected by the V/A ratio.
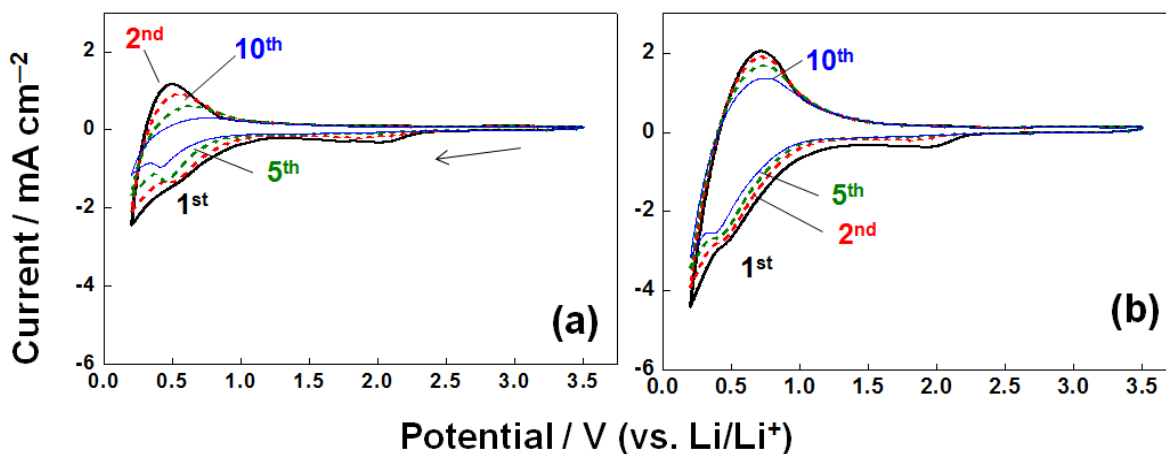
Fig. 9. CVs of (a) thin (2.1 mg/cm^2) and (b) thick (9.4 mg/cm^2) graphite composite electrodes in 1 M LiPF$_6$ EC/DEC (1/2, v/v) solution.

3.1.3 XPS

The chemical compositions of the SEI layer on the thin and thick electrodes tested in Fig. 10 were examined by using X-ray photoelectron spectroscopy (XPS) measurements. The thin and thick electrodes exhibit quite different Li1s and F1s spectra, while showing similar C1s and O1s spectra. According to previous XPS studies on graphite anodes [30-32], peak assignment can be made as follows: F 1s peak at 685 eV is assigned to LiF and the peak at 687 eV to LiPF$_6$-derived products (LiPF$_6$/LiP$_x$F$_y$O$_z$). The Li 1s spectrum for thin electrode shows a LiF peak at 55.5 eV and Li$_2$CO$_3$ peak at 54.5 eV. The C 1s peaks at 284, 285, 286.5, 287.8, 288.5, and 290 eV are attributed to graphite, hydrocarbon, C-O, O-C-O, O-C=O, and Li$_2$CO$_3$, respectively. The O 1s peaks at 532 and 533 eV are assigned to O-C=O/Li$_2$CO$_3$ or C-O/ O-C-O, respectively. Atomic composition of the SEI layers is compared in Table 1. F and Li are the most abundant elements for the SEI of the thin electrode. On the other hand, F and Li contents are quite reduced while C and O portions

are increased in the thick electrode. In brief, inorganic LiF and salt-derived product are major constituents of the SEI of thin electrode, whereas the SEI of thick electrode mainly consists of solvent reduction product such as ROCO$_2$Li. Note that LiF portion in the SEI of thin electrode is more than three times larger than that in the thin electrode (Table 1). Previously, we revealed that HF present in LiPF$_6$ solution is electrochemically reduced to form a LiF layer on a Pt surface, which hampers further cathodic reactions of the solvent species [32]. Aurbach et al. also observed HF-induced LiF formation on graphite surface, and reveled that the LiF film on the graphite composite electrode [30] acts as a barrier for Li$^+$ transport. Therefore, it can be concluded that the rapid capacity fading observed in thin electrode is ascribed to the high LiF content, which is presumably induced by HF reduction on the electrode surface.
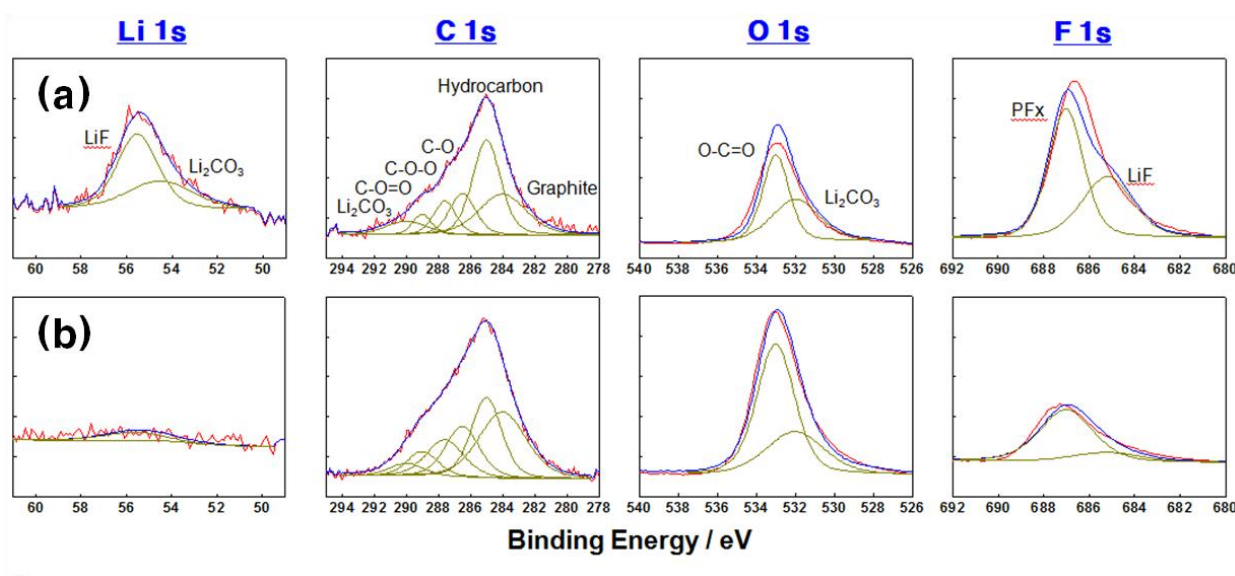
Fig. 10. XPS spectra for the graphite composite electrodes subjected to ten CV cycles over 0.2–3.5 V in 1 M LiPF$_6$ EC/DEC (1/2, v/v) solution. (a) thin and (b) thick graphite composite electrodes.

Graphite electrode	F (LiF)	F (LiP$_x$F$_y$O$_z$)	Li	C	O
Thin	20	28	27	7	18
Thick	6	26	8	14	46

Table 1. Atomic percentages derived from XPS measurements in Fig. 10.

3.1.4 Area comparison by double-layer capacitances (C_{dl}) of emery-PGE and alumina-PGE

Emery-PGE and alumina-PGE surface area was estimated by double-layer capacitance, C_{dl} which is related to fraction of electrochemical active site, edge plane on PGE. Fig. 11 shows a C_{dl} was measured by cyclic voltammogram with emery-PGE and alumina-PGE in 1.0M KCl solution with a Ag/AgCl reference and platinum counter electrode. Scan rate ranges were increased from 500 to 5000 mV/s. Fig. 11a is CVs of emery-PGE and Fig. 11b is CVs of alumina-PGE. Steady-state currents of emery-PGE are greater than alumina-PGE by increased scan rate. The slope of the steady-state current versus scan rate gives the double layer capacitance which is shown in Fig. 11c.
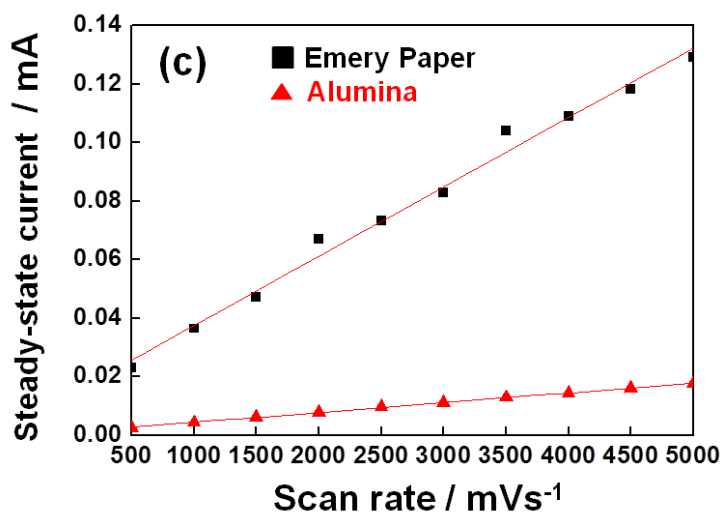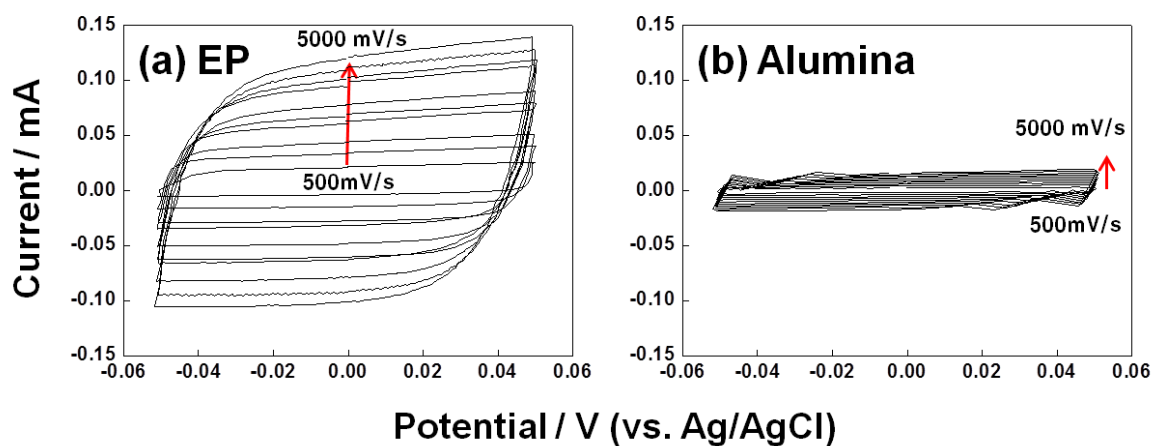
Fig. 11. CVs of (a) emery paper polished PGE, (b) alumina polished PGE in 1M KCl, scan rate from 500 m Vs^{-1} to 5,000 mVs^{-1} within the potential range of -5 mV to 5 mV (vs. Ag/AgCl). (c) Slopes of the steady-state current versus scan rate: emery paper (■), alumina (▲).

The slope of the steady-state current is related to f_e by

$$C_{dl} = C_{dl,e}\,f_e + C_{dl,b}(1 - f_e) \qquad [1]$$

The values for $C_{dl,e}$ and $C_{dl,b}$ used were 60 and 2 μF/cm^2 [33, 34]. C_{dl} of emery-PGE is 333 μF/cm^2 and C_{dl} of alumina-PGE is 48 μF/cm^2 which were calculated by the slope of the steady-state current of each polishing conditions from Fig. 11c. f_e of emery-PGE and alumina-PGE as calculated from Eq. 1 is shown in Table. 2. The f_e of emery-PGE is 5.7 which is 7.2 times than f_e of alumina-PGE, 0.79. This result indicated that active site of emery-PGE has at least 7 times more than alumina-PGE. Therefore changing polishing method affects a lot the V/A area ratio by its f_e.

	Emery-PGE	Alumina-PGE
C_{dl} (μF/cm^2)	333	48
fraction of edge (f_e)	5.7	0.79

Table 2. Double-layer capacitance (C_{dl}) and fraction of edge (f_e) of emery-PGE and alumina-PGE.

3.1.5 Proposed mechanism dependence on the V/A ratio

The possible explanation for the observed Li$^+$ ion transport of graphite anode in a LiPF$_6$ solution is schematized in Fig. 12. When the V/A ratio is high (Fig. 12a), LiF-rich SEI, which suppresses Li$^+$ transport more than organic-abundant SEI, is formed on graphite surface. The formation LiF is determined by the absolute amount of HF present in the electrolyte, and thus the overall thickness of the surface LiF layer is proportional to the V/A ratio. Therefore, if the V/A ratio is lowered either by increasing electrode surface area (Fig. 12b) or by decreasing electrolyte volume (Fig. 12c), then thinner LiF layer would be formed so that facile Li$^+$ transport can be achieved.

Since the commercial LIBs have much lower electrolyte volume to electrode area ratio, the HF effects are less pronounced than in the flooded cells commonly adopted for HOPG experiments.
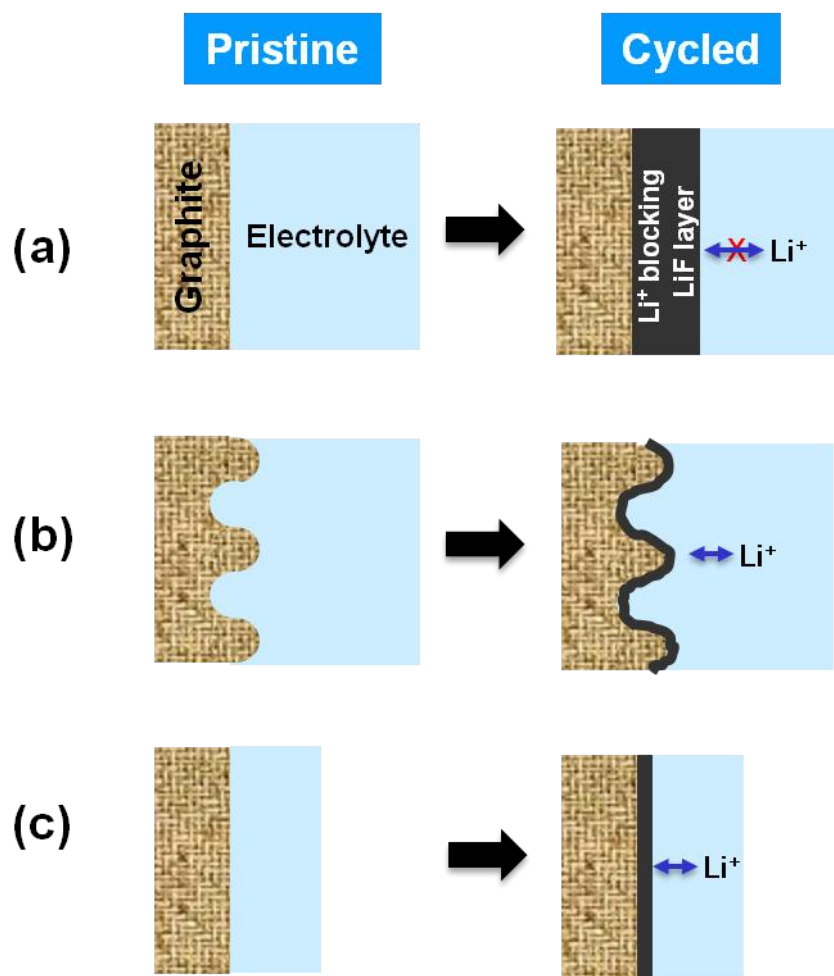
Fig. 12. Schematic diagram of the Li$^+$ ion transport of graphite anode in a LiPF$_6$ solution. (a) the V/A ratio is high, and thus the Li$^+$ ion transport is suppressed. The ratio is low (b) due to increased electrode area, and (c) due to decreased electrolyte volume, enabling facile Li$^+$ ion transport.

3.1.6 Comparison theoretical capacity with experimental capacity of graphite composite

It needs to be checked capacity that theoretical value matched up practical one of artificial graphite composite. Theoretical capacity of thin graphite composite is 0.15 mAh on 0.25cm^2 (size: 5 x 5 mm) and thick one is 0.54 mAh in Fig. 9. Table. 3 shows practical capacity and efficiency of thin and thick electrodes during CV measurements until 10cycles in Fig 9. The practical capacities are much smaller than theoretical ones. There are too much gaps with practical between theoretical capacities.

	Thin (0.15 mAh)			Thick (0.54 mAh)		
	1st cycle	2nd cycle	10th cycle	1st cycle	2nd cycle	10th cycle
Charge capacity (mAh)	0.02	0.016	0.009	0.036	0.029	0.023
Discharge capacity (mAh)	0.01	0.009	0.005	0.02	0.019	0.016
Efficiency (%)	51	57	58	54	65	70

Table 3. Practical capacities and efficiencies of thin and thick electrodes during CVs from Fig. 9 (scan rate: 5 mVs^{-1}).

Since the scan rates of those experiments were too fast than coin cell experiments, slower scan rate (0.5mV/s) CVs were examined to measure more exactly. The CVs are shown in Fig. 13. The current of CVs were decreased because of slow scan rate, 0.5mV/s in Fig. 13 which is less 10 times than Fig. 9. Despite slow scan rate, the practical capacities are not matched the theoretical ones since these examination condition is not the same with real condition like coin cell until 5mV (vs. Li/Li$^+$).
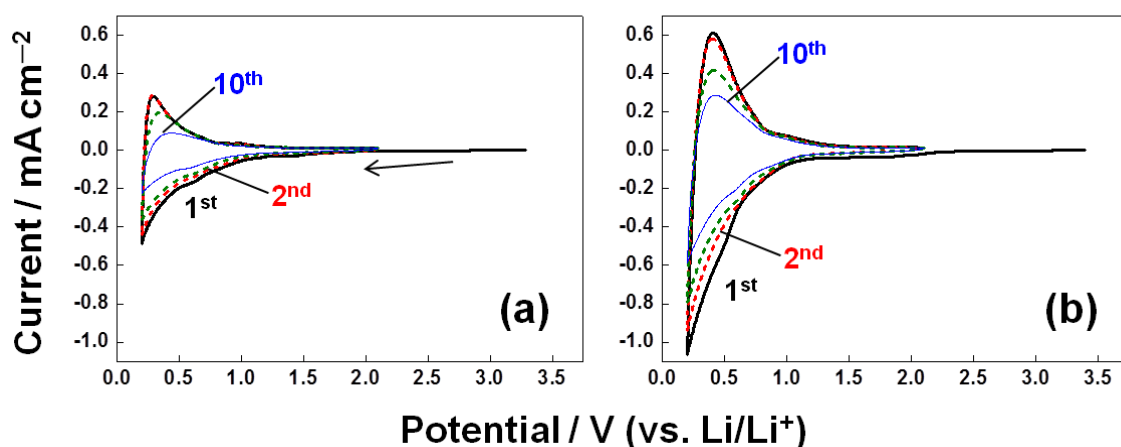
Fig. 13. CVs of (a) thin (0.15 mAh) and (b) thick (0.54 mAh) graphite composite electrodes in 1 M LiPF$_6$ EC/DEC (1/2, v/v) solution at scan rate 0.5 mVs^{-1}.

Table. 4 shows practical capacity and efficiency of thin and thick electrodes during CV measurements until 10cycles in Fig 13. Capacities and efficiencies are improved than fast scan rate (5mV/s, in Fig. 9) but not significantly.

	Thin (0.15 mAh)			Thick (0.54 mAh)		
	1st cycle	2nd cycle	10th cycle	1st cycle	2nd cycle	10th cycle
Charge capacity (mAh)	0.026	0.021	0.012	0.056	0.044	0.03
Discharge capacity (mAh)	0.015	0.014	0.0077	0.035	0.033	0.02
Efficiency (%)	57	69	62	61	75	68

Table 4. Practical capacities and efficiencies of thin and thick electrodes during CVs from Fig. 10 (scan rate: 0.5 mVs^{-1}).

3.2. Mg-ion battery

3.2.1 Searching for reversible Mg electrolyte

The early part of investigation, various Mg mixture solutions were carried out for Mg battery electrolytes. Fig. 14 shows CVs which have Mg deposition/dissolution reaction using Mg bis(diisopropyl) amide solution (0.7 M THF) (the structure is shown inset of Fig. 14b) among one of those solutions invested. It was first evaluated by CV using a three electrode configuration; Mg strips were used for working, reference and counter electrode. As shown Fig. 14a, there is overpotential (about -0.4 V) during deposition process but Mg working electrode allowed Mg deposition/dissolution reaction in this solution. Therefore, Pt electrode was also invested CV. Pt delivered lower efficiency than Mg for the Mg deposition/dissolution process (Fig 14b). This solution gave one of possibility using not Grignard reagent. The efficiency of Mg and Pt electrode for Mg deposition/dissolution is shown table 5, 169 % and 32 %, respectively.

However, Mg bis(diisopropyl) amide solution (0.7 M THF) is so sensitive so that the reversibility was not guaranteed for Mg battery electrolyte. Therefore we tried to find new concept of electrolyte for Mg bat-

teries.
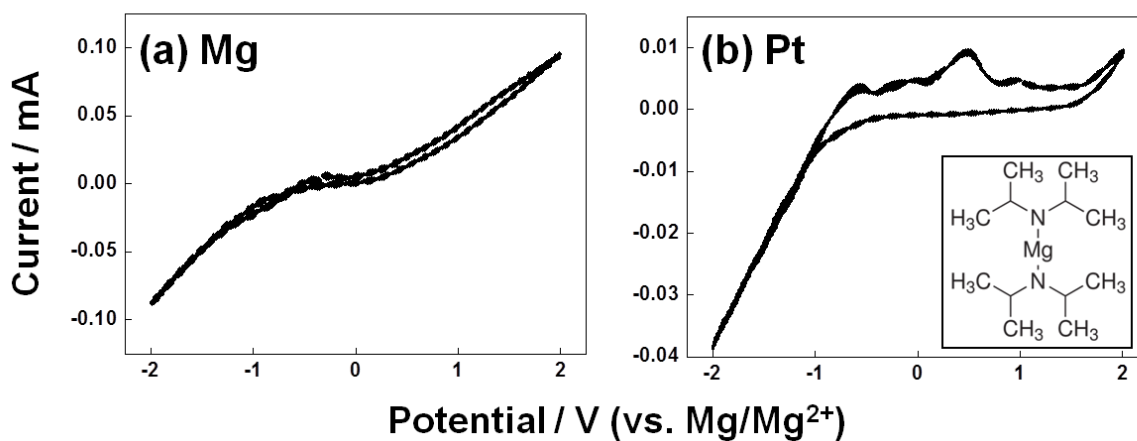
Fig. 14. CVs of (a) Mg working and (b) Pt working electrode in Mg bis(diisopropyl) amide solution (0.7 M

THF) electrolyte at scan rate 20 mVs^{-1} and structure of Mg bis(diisopropyl) amide solution (inset).

Electrode	Mg	Pt
Deposition	5.04 mC	0.958 mC
Dissolution	8.50 mC	0.306 mC
Efficiency	169%	32%

Table 5. Deposition / dissolution efficiency of Mg bis(diisopropyl) amide solution (0.7M THF) electrolyte

on Mg and Pt electrodes.

3.2.2 Dialkyl sulfone-based electrolytes

Sulfone electrolytes such as dimethyl sulfone (DMSO$_2$) were known as electrodepositing electrolytes

for aluminum deposition based on $AlCl_3$ salt, L. LEGRAND et al.[35] Adopting the concepts, electrolyte based on $MgCl_2$ / sulfone mixture were invested for rechargeable Mg batteries systems. However, since melting point of $DMSO_2$ is over 100°C, CV experiment is not able to be operated in room temperature. It is necessary that sulfones have lower melting point or adding co-solvent that are able to be used system solution around room temperature. Ethyl methyl sulfone ($EMSO_2$), dipropyl sulfone ($DPSO_2$) and dibutyl sulfone ($DBSO_2$) are appropriate candidates near room temperature system (Table 6).

	Dimethyl ($DMSO_2$)	Ethylmethyl ($EMSO_2$)	Dipropyl ($DPSO_2$)	Dibutyl ($DBSO_2$)
mp (°C)	107-109	32-37	29-33	43-45

Table 6. Melting points of sulfones.

Fig. 15 shows a cyclic voltammogram measured with Pt and GC electrode as a working electrode in $EMSO_2$ solution containing 2M $MgCl_2$ on 45 °C and 65 °C, respectively. Mg deposition/dissolution is not prominent on Pt electrode at 45 °C (Fig. 15a). However increasing temperature to 65 °C and changing electrode to GC were enhanced Mg deposition/dissolution (Fig. 15b, c, d). In addition, electrochemical window of $EMSO_2$ solution is as large as Grignard reagents which are stable electrochemically up to 3.1 V.
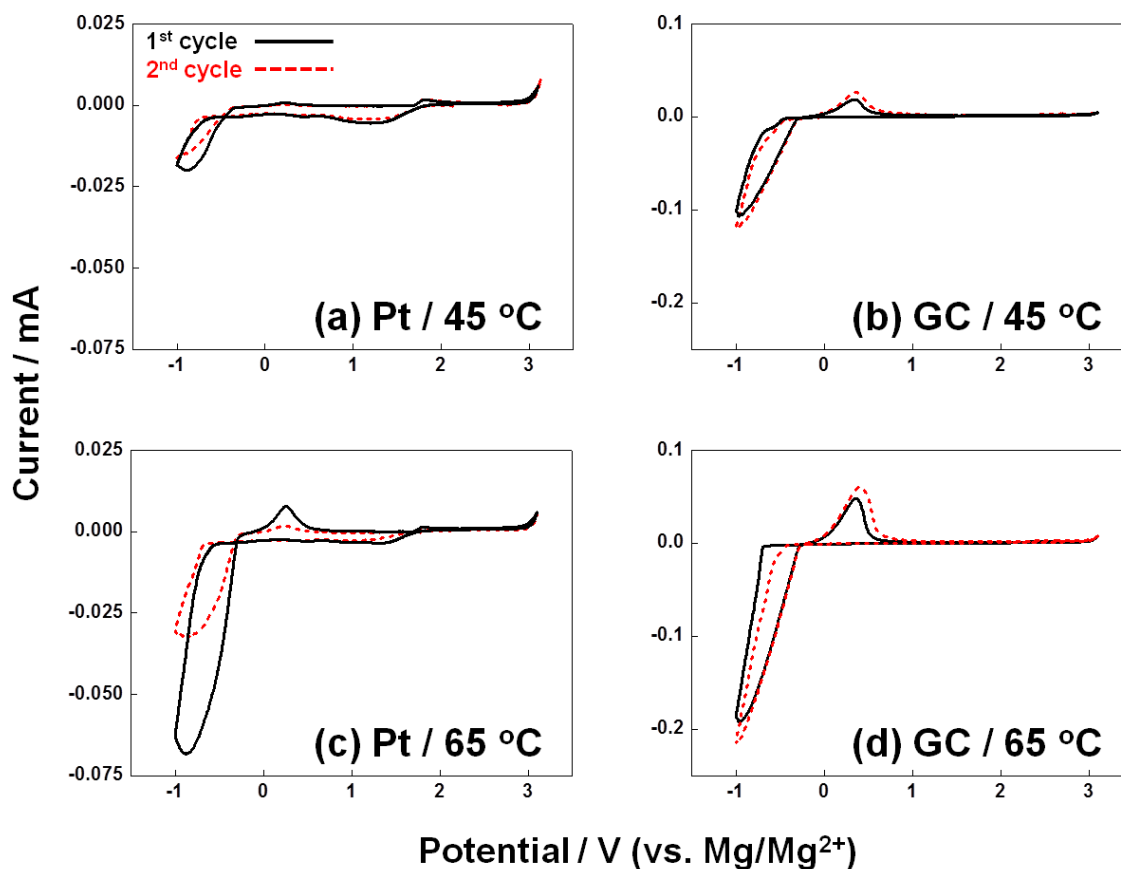
Fig. 15. CVs showing magnesium deposition/dissolution on (a) Pt electrode, 45 °C (b) GC, 45 °C (c) Pt, 65 °C and (d) GC, 65 °C in 2M MgCl$_2$ / EMSO$_2$ electrolyte at a voltage scan rate of 10mVs^{-1} within the potential range of -1 to 3.1 V (vs. Mg/Mg^{2+})

Mg deposition/dissolution was proved in DPSO$_2$ solution than EPSO$_2$ in Fig. 16. Despite of lower temperature at 35 °C from 45 °C which the temperature of EMSO$_2$ experiments were taken, deposition/dissolution behaviors were shown more clearly (Fig. 16a, b). We assume this phenomenon is related to its lower melting point than EMSO$_2$. As the same reason, DBSO$_2$ solution (mp. 43-45 °C, Table 6) didn't show Mg deposition/dissolution behaviors even though at 60 °C state (Fig. 17a, b). Furthermore, electrolyte was solidified after CV experiments. (Fig. 17c)

Among those electrolyte systems, DPSO$_2$ solution has fair deposition/dissolution efficiency and elec-

trochemical properties.
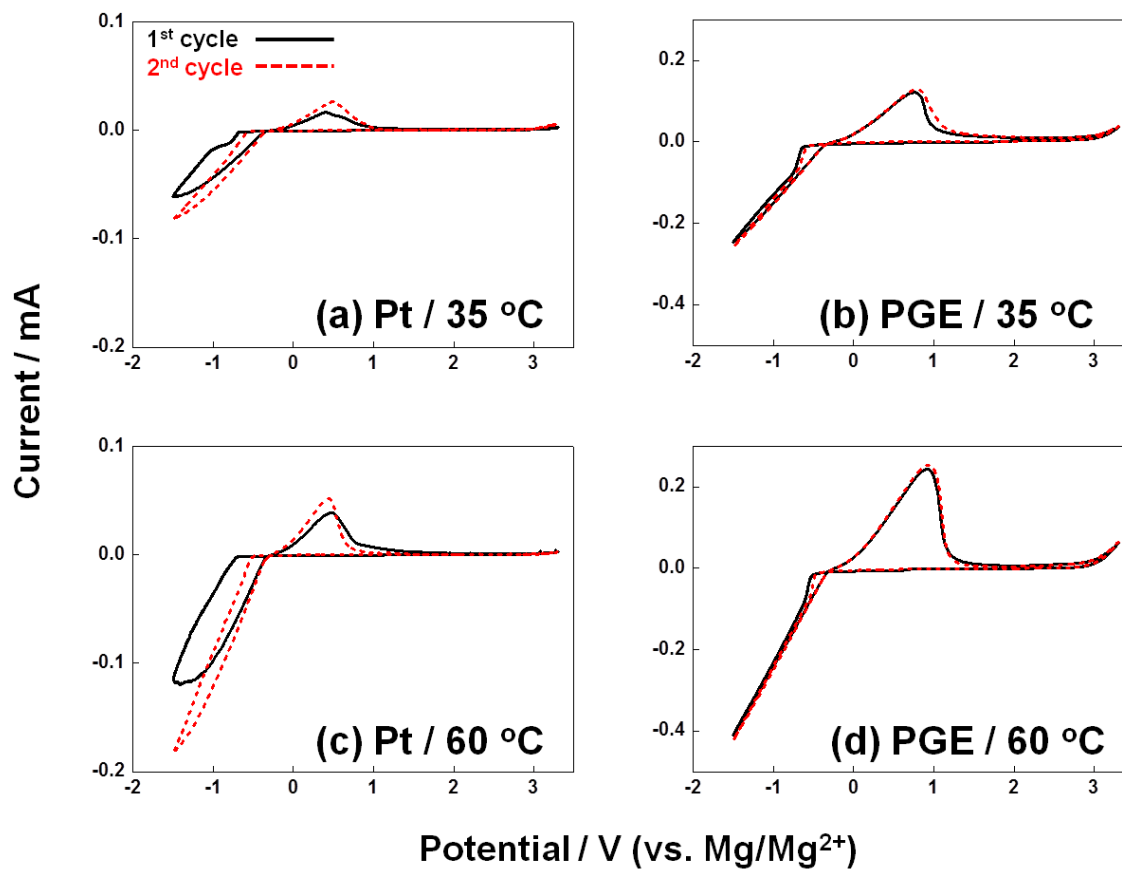
Fig. 16. CV of 1M MgCl$_2$ / DPSO$_2$ electrolyte on (a) Pt electrode, 35 ^{o}C (b) PGE, 35 ^{o}C (c) Pt, 60 ^{o}C and (d) PGE, 60 ^{o}C in at a voltage scan rate of 20mVs^{-1} within the potential range of -1.5 to 3.3 V (vs. Mg/Mg^{2+})
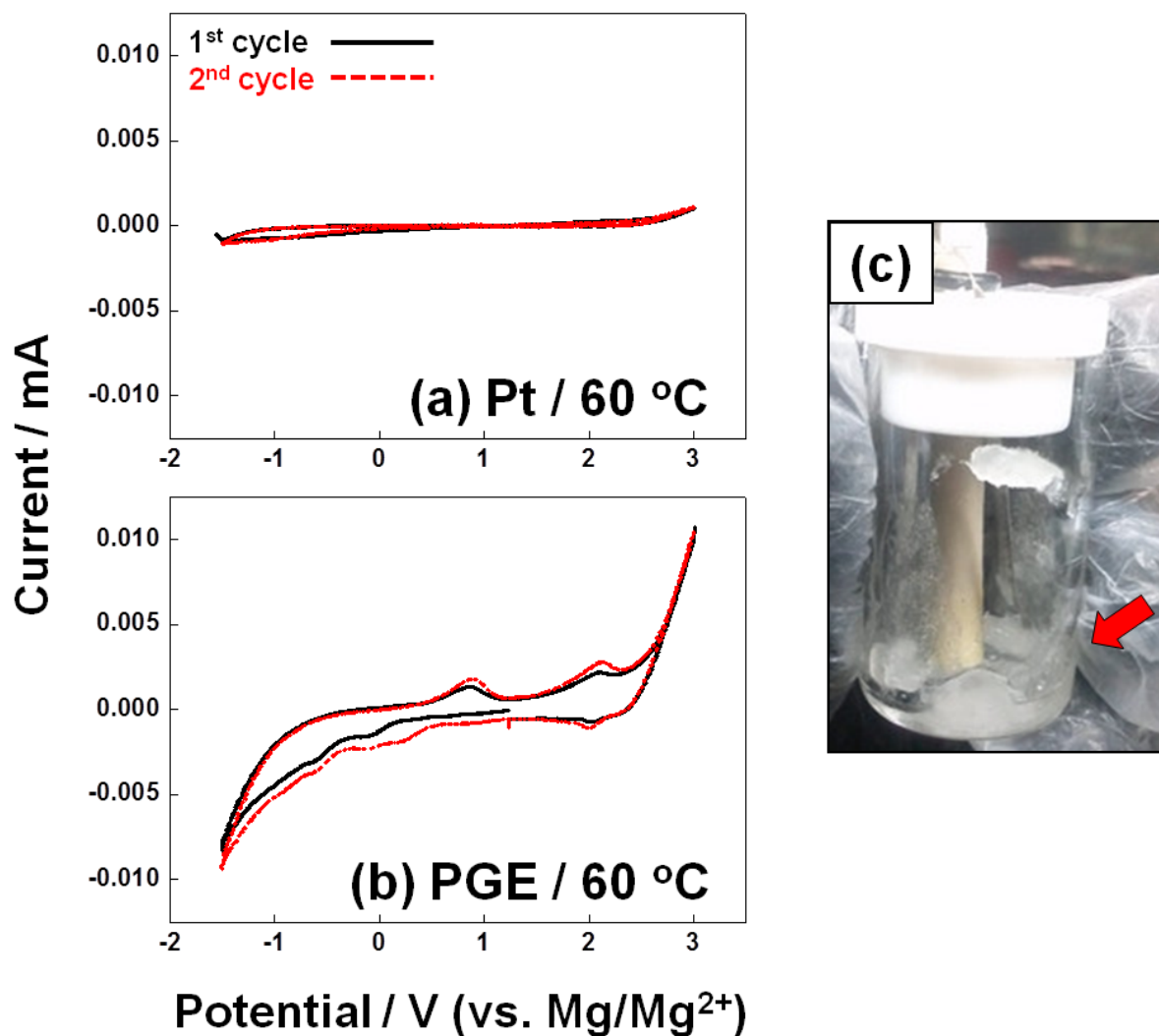
Fig. 17. CV of 1M MgCl$_2$ / DBSO$_2$ electrolyte on (a) Pt electrode, 60 ^{o}C and (b) PGE, 60 ^{o}C in at a voltage scan rate of 20mVs^{-1} within the potential range of -1.5 to 3 V (vs. Mg/Mg^{2+}). (c) After CV experiment in 3-electrode configuration, electrolyte was solidified (red arrow).

There were other experiments of sulfone-based electrolytes which were used alone for host solvent of Mg rechargeable batteries. Unfortunately, we were not able to find possible solvent systems for Mg electrolyte, expect EMSO$_2$ and DPSO$_2$. Ethyl isopropyl sulfone (EiPSO$_2$), methyl isopropyl sulfone (MiPSO$_2$),

ethyl phenyl sulfone (EPSO$_2$) and Dimethyl sulfite (DMSO) were invested. Table 7 shows efficiencies of singular sulfone-based electrolyte above solvents.

Components	Temp. (℃)	Working electrode	Efficiency (%)	
			1st cycle	2nd cycle
2M MgCl$_2$ EMSO$_2$	65	Pt	4.2	11
		Edge	24	32
1M MgCl$_2$ EiPSO$_2$	No deposition/dissolution reaction			
1M MgCl$_2$ MiPSO$_2$	No deposition/dissolution reaction			
1M MgCl$_2$ DBSO$_2$	No deposition/dissolution reaction			
1M MgCl$_2$ EPSO$_2$	No deposition/dissolution reaction			
0.05M MgCl$_2$ DMSO	No deposition/dissolution reaction			
1M MgCl$_2$ DPSO$_2$	35	Pt	17.5	17.3
		Edge	33.2	36.7
	60	Pt	20.7	12.4
		Edge	37.5	37.2

Table 7. Efficiencies of singular sulfone-based electrolyte.

3.2.3 Eutectic: dialkyl sulfones used for co-solvent electrolyte

Although Mg deposition/dissolution is obtained in sulfone solution with MgCl$_2$ salt, its efficiency is not affordable for battery systems. Therefore, new attempts were needed to improve the efficiency of Mg electrolyte system, such as fabricating eutectic and mixture with other sulfones. Here, various mixtures were carried out for Mg electrolyte system.

A 3:1 solution of EMSO$_2$ and DMSO$_2$ has a eutectic temperature of 23 ^{o}C. This solution was invested

for new electrolyte for Li rechargeable battery by Angell group.[36] Adopting this concept from Angell group, $EMSO_2$ / $DMSO_2$ (3/1) eutectic was used for solvent with $MgCl_2$ salt. Since $EMSO_2$, $DMSO_2$ and $MgCl_2$ are all solid state in room temperature, electrolyte was mixed each salt by per mole weight: $MgCl_2$, $EMSO_2$ and $DMSO_2$ are 0.35, 3 and 1 weight percent, respectively. Fig. 18 shows CVs of $MgCl_2$/$EMSO_2$/$DMSO_2$ (0.35/3/1, wt %) eutectic electrolyte. Current magnitudes and efficiency of $MgCl_2$/$EMSO_2$/$DMSO_2$ (0.35/3/1, wt %) eutectic were improved than singular solvents which were used each $EMSO_2$ (Fig. 15) or $DMSO_2$.
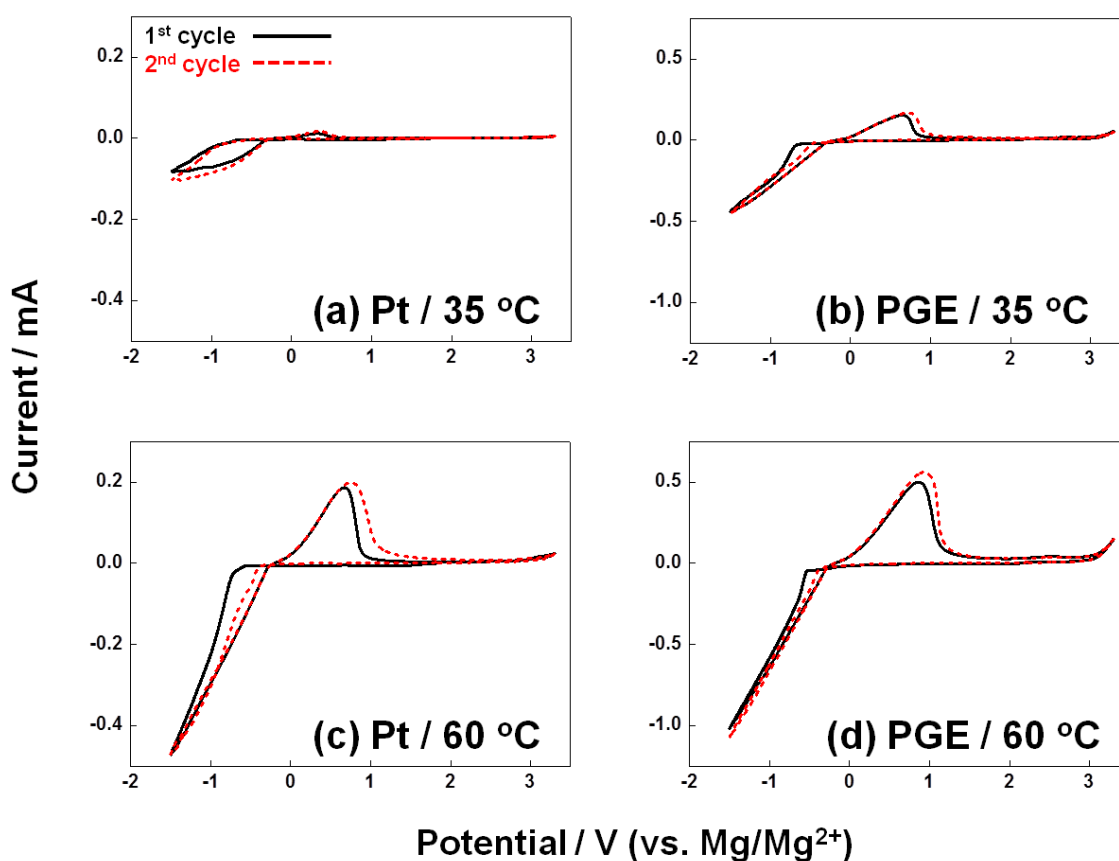
Fig. 18. CV of $MgCl_2$ / $EMSO_2$ / $DMSO_2$ (0.35/3/1, wt %) eutectic electrolyte on (a) Pt electrode, 35 °C (b) PGE, 35 °C (c) Pt, 60 °C and (d) PGE, 60 °C in at a voltage scan rate of $20 mVs^{-1}$ within the potential range of -1.5 to 3.3 V and 3.5 V (vs. Mg/Mg^{2+}).

A 1:1 solution of $EMSO_2$ and $DBSO_2$ was invested for Mg electrolyte and the results of CV is shown in Fig. 19. Deposition/dissolution reaction was not shown when $DBSO_2$ was used singular solvent (Fig. 17). However, this $EMSO_2/DBSO_2$ (1/1 vol) eutectic solvent does not solidify in 35 ^oC. In addition, current magnitudes and efficiency of $EMSO_2/DBSO_2$ (1/1 vol) eutectic solvent were improved than singular solvent of $DBSO_2$ (Fig. 17).

Fig. 19. CV of 1M $MgCl_2$ / $EMSO_2$ + $DBSO_2$ (1/1, vol %) eutectic electrolyte on (a) Pt electrode, 35 ^oC (b) PGE, 35 ^oC (c) Pt, 60 ^oC and (d) PGE, 60 ^oC in at a voltage scan rate of 20mVs^{-1} within the potential range of -1.5 to 3.3 V and 3.5 V (vs. Mg/Mg^{2+}).

Fig. 20 shows CVs of DPSO$_2$ and DBSO$_2$ mixture of 1:1 volume ratio. DPSO2/DBSO2 (1/1) solution does not become low temperature eutectic. Therefore this mixture was able to be carried only in 60 ^{o}C, not 35 ^{o}C in Fig. 20.
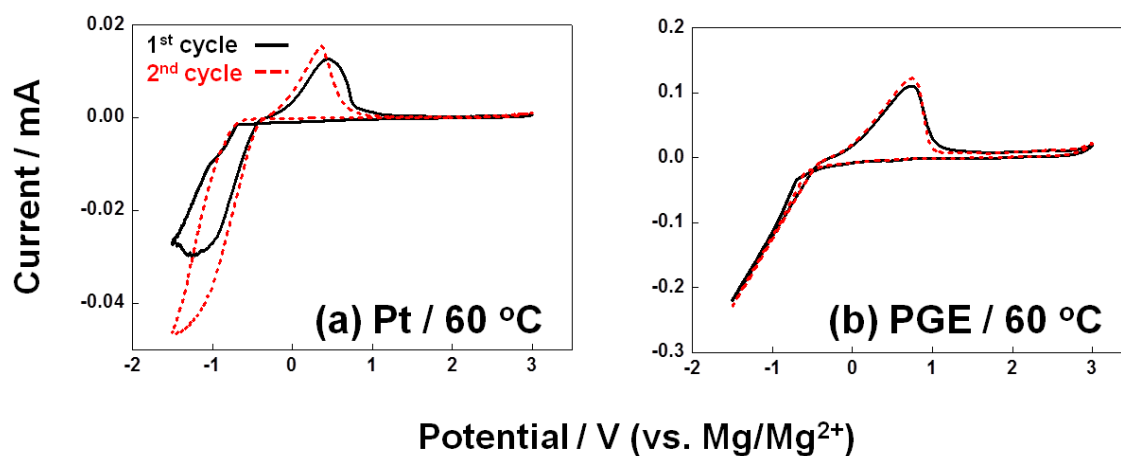
Fig. 20. CV of 1M MgCl$_2$ / DPSO$_2$ + DBSO$_2$ (1/1, vol %) electrolyte on (a) Pt electrode, 60 ^{o}C and (b) PGE, 60 ^{o}C in at a voltage scan rate of 20mVs^{-1} within the potential range of -1.5 to 3 V (vs. Mg/Mg^{2+}).

There were other experiments of sulfone-based eutectic electrolytes. Various sulfone mixture eutectics were invested. The efficiencies of those eutectics were presented in Table 8.

Components	Temp. (℃)	Working	Efficiency (%)	
			1st cycle	2nd cycle
2M MgCl$_2$ EMSO$_2$/DPSO$_2$ (3/1, vol)			No deposition/dissolution reaction	
1M MgCl$_2$ DPSO$_2$/EiPSO$_2$ (1/1, vol)	25	Pt	6	7
		Edge	32	31
1M MgCl$_2$ DBSO$_2$/EiPSO$_2$ (1/1, vol)			No deposition/dissolution reaction	
1M MgCl$_2$ DPSO$_2$/DBSO$_2$ (1/1, vol)	35		No deposition/dissolution reaction	
	60	Pt	23	16
		Edge	33	33
1M MgCl$_2$ EMSO$_2$/DBSO$_2$ (1/1, vol)	35	Pt	20	22
		Edge	20	22
	60	Pt	8	8.6
		Edge	34	39
0.8M MgCl$_2$ DPSO$_2$/EMSO$_2$ (3/1, vol)	35	Pt	5.2	5.1
		Edge	No deposition/dissolution reaction	
	60	Pt	5.5	6.8
		Edge	29	33
MgCl$_2$/EMSO$_2$/DMSO$_2$ (0.35/3/1, wt)	35	Pt	5.7	7
		Edge	19	23
	60	Pt	20	26
		Edge	30	33

Table 8. Efficiencies of sulfone-based eutectic electrolyte.

3.2.4 Dialkyl sulfones with THF (1/1, vol) electrolyte

Fig. 21 shows cyclic voltammogram with sulfones with THF (1/1, vol) solution containing 0.8M MgCl$_2$. Currents of Mg deposition/dissolution are significantly improved than using sulfones alone or eutectics. Especially, the efficiencies and current magnitude of DPSO$_2$ and DBSO$_2$ with THF were increased

dramatically than previous experiment of DPSO2 (Fig. 16, 17).
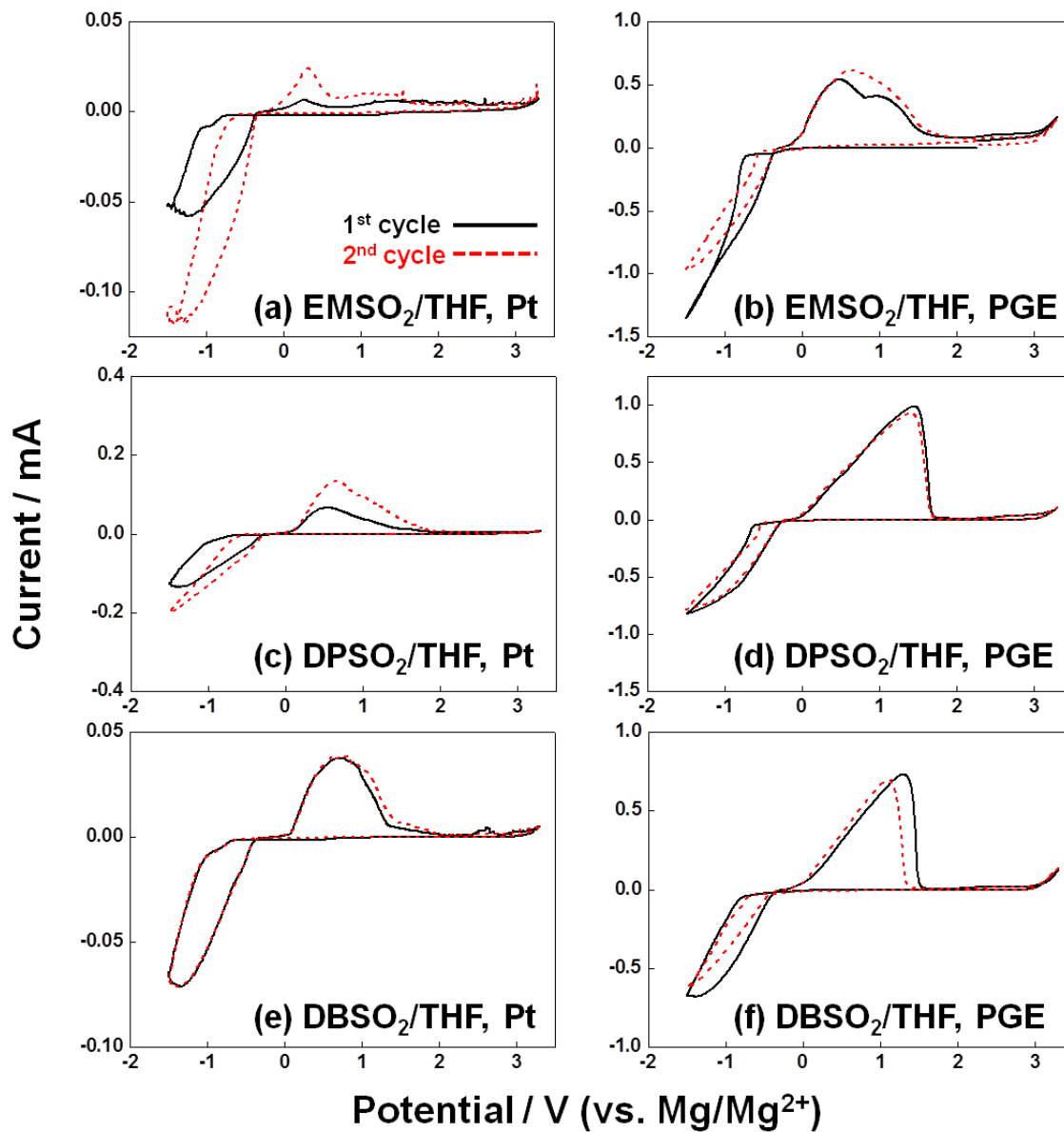
Fig. 21. CV of sulfones with THF (1/1, vol) electrolyte containing 0.8M MgCl₂. (a) EMSO₂/THF on Pt electrode, (b) EMSO₂/THF on PGE, (c) DPSO₂/THF on Pt, (d) DPSO₂/THF on PGE, (e) DBSO₂/THF on Pt, and (f) DBSO₂/THF on PGE in at a voltage scan rate of 20mVs⁻¹ within the potential range of -1.5 to 3.3 V (vs. Mg/Mg²⁺) at 30 °C

Table 9 shows efficiencies of sulfones / THF (1/1, vol) electrolyte. The efficiency of DPSO$_2$/THF is increased from 17 to 44 % on Pt and from 33 to 85 % (Table 7, 9). It is presented that the efficiencies of these complexes with THF are increased when those alkyl chains are increasing; EMSO$_2$ < DPSO$_2$ < DBSO$_2$. The phenomena are seemed to be related with forming solvated Mg complexes with sulfone and THF solvents. This need to be clarified next study.

Components	Temp. (℃)	Working	Efficiency (%)	
			1st cycle	2nd cycle
0.8M MgCl$_2$ EMSO$_2$/THF (1/1, vol)	30	Pt	17	15
		Edge	44	69
0.8M MgCl$_2$ DPSO$_2$/THF (1/1, vol)	30	Pt	44	57
		Edge	85	85
0.8M MgCl$_2$ DBSO$_2$/THF (1/1, vol)	30	Pt	50	57
		Edge	84	83

Table 9. Efficiencies of EMSO2, DPSO2 and DBSO2 with THF (1/1, vol) electrolyte.

3.2.5 Comparison efficiencies with volume changing of DPSO$_2$ and THF

We compared efficiencies dependent on the volume ratio changing of DPSO$_2$ and THF because DPSO$_2$/THF complex was shown the highest current and efficiency in our studies. Fig. 22 shows CVs of each case of DPSO$_2$/THF complex, such as 1/1, 1/2 and 2/1. The deposition/dissolution reaction and columbic efficiency are dominant when each solvent, DPSO$_2$ and THF is same volume rate; 1/1. The efficiencies are checked in table 10.
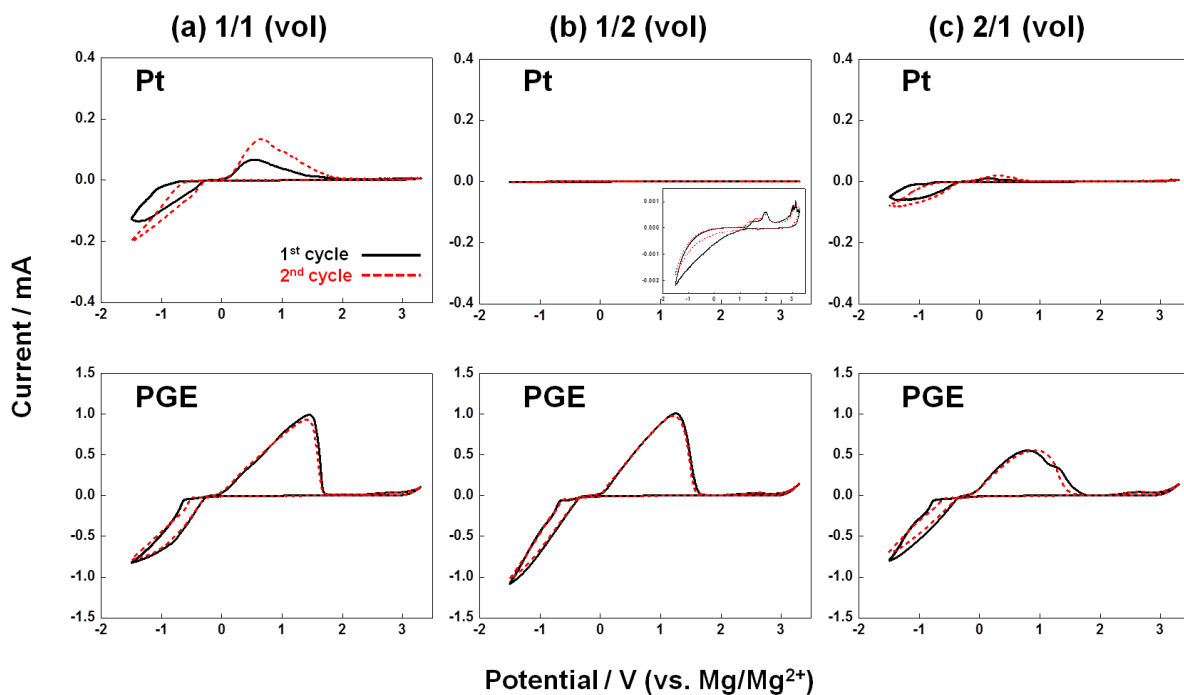
Fig. 22. CV of DPSO$_2$/THF electrolyte containing 0.8M MgCl$_2$ volume ratio (a) 1:1, (b) 1:2, (c) 2:1 of DPSO$_2$/THF on Pt and PGE at 30 ^{o}C in at a voltage scan rate of 20mVs^{-1} within the potential range of -1.5 to 3.3 V (vs. Mg/Mg^{2+})

Vol. ratio (DPSO$_2$/THF)			1 / 1	1 / 2	2 / 1
30℃	Pt	1st	44 %	No reaction	9 %
		2nd	57 %		13 %
	Edge	1st	85 %	79 %	69 %
		2nd	85 %	80 %	71 %
60℃	Pt	1st	32 %	31 %	4 %
		2nd	48 %	28 %	10 %
	Edge	1st	82 %	76 %	30 %
		2nd	81 %	76 %	37 %

Table 10. Efficiency of DPSO$_2$/THF dependant on volume ratio (v/v) on Pt and Edge electrodes at 30 ^{o}C and 60 ^{o}C.

3.2.6 Characteristics of DPSO$_2$ vs. DPSO$_2$/THF (1/1) and ionic conductivity

DPSO$_2$/THF, the highest efficiency among above sulfones was 1 to 1 volume ratio. Therefore it needed to be investigated what affect efficiencies with adding tetrahydrofuran (THF). Here the characteristics of DPSO$_2$ and DPSO$_2$ / THF (1/1) were compared with ionic conductivity.

Deposition / dissolution efficiency of DPSO$_2$/THF (1/1) mixture electrolyte is over 80% on PGE electrode (Table. 11). Efficiencies of DPSO$_2$ used alone present around 12 to 20% both Pt and PGE electrodes. On the other hand, the efficiencies on Pt electrode are 3times (43.7 and 56.5 %) and on PGE electrode are 4 times (84.6 and 85.1 %) than using single DPSO$_2$ at 31 ^{o}C.

This different tendency is related to ionic conductivity of each solution since viscosity is decreased adding THF in DPSO$_2$ solution. Ionic conductivities of DPSO$_2$ and DPSO$_2$/THF containing 0.8M MgCl$_2$ are shown at Fig. 23. Conductivity of DPSO$_2$/THF was measured from 10 ^{o}C to 80 ^{o}C by each 10 ^{o}C. Conductivity of only DPSO$_2$ was measured from 30 ^{o}C because it was frozen when below 25 ^{o}C due to its melting point (29-33 ^{o}C, Table 6).

		Pt		Edge	
	Cycle	35℃	60℃	35℃	60℃
Only DPSO$_2$	1st	17.5%	20.7%	17.5%	20.7%
	2nd	17.3%	12.4%	17.3%	12.4%
DPSO$_2$ / THF(1/1)	1st	43.7%	31.8%	84.6%	81.9%
	2nd	56.5%	47.7%	85.1%	80.3%

Table 11. Efficiency of DPSO$_2$ alone and DPSO$_2$/THF (1/1, v/v) on Pt and Edge electrodes.
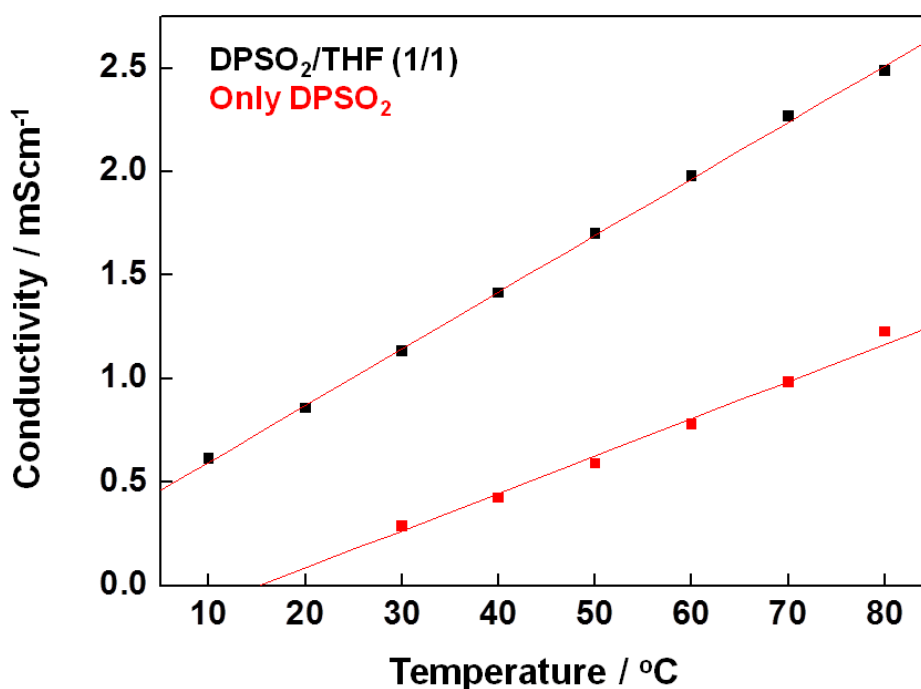
Fig. 23. Ionic conductivities of DPSO$_2$/THF and DPSO$_2$ electrolyte containing 0.8M MgCl$_2$ Measurement range of DPSO$_2$/THF was from 10 to 80 ^{o}C and DPSO$_2$ was from 30 to 80 ^{o}C.

3.2.7 CVs and coin cell test of Chevrel phase cathode electrode with DPSO$_2$/THF solution

CV was performed on a well-known Mg intercalation material Mo$_6$O$_8$ Chevrel phase cathode electrode in DPSO$_2$/THF containing 0.8M MgCl$_2$ electrolyte in at a voltage scan rate of 0.1mVs^{-1} within the potential range of 0 to 2.1 V (vs. Mg/Mg^{2+}). CV shows highly reversible Mg intercalation/de-intercalation in DPSO$_2$/THF solution. The process of Mg insertion into Chevrel phase takes two stages due to its structure morphology.[20] The first stage of intercalation (sites A in Fig. 24) is indicated around 0.8 – 0.9V and the another one is indicated around 0.6V.
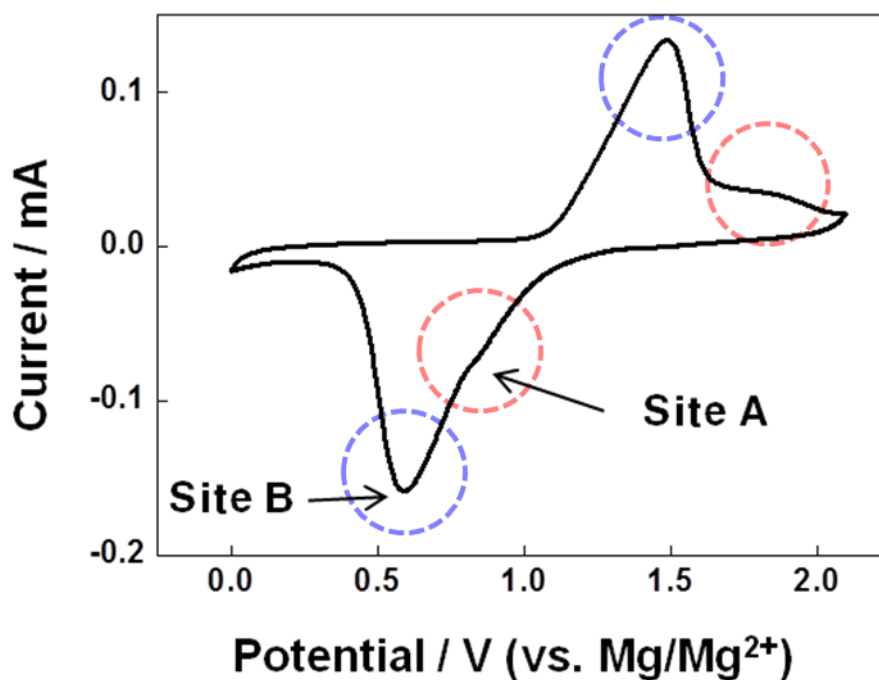
Fig. 24. CV of DPSO$_2$/THF electrolyte containing 0.8M MgCl$_2$ on Chevrel phase cathode in at a voltage scan rate of 0.1mVs^{-1} within the potential range of 0 to 2.1 V (vs. Mg/Mg^{2+})

Fig. 25 and 26 show the coin cell test of Mg with DPSO$_2$/THF (1/1). The result of 3 electrode configuration CVs were quite reversible. The Mg coin cell which consists of Mg metal anode, DPSO$_2$/THF (1/1, vol) and Mo$_6$S$_8$ cathode delivers at a 0.2 C rate; the capacity drops slightly but it stays around 96% capacity (Fig. 25c). These indicate DPSO$_2$/THF (1/1) electrolyte is able to support reversible Mg^{2+} insertion/deinsertion in cathode material and the cycling is stable. In the other hand, Mg/Pt coin cell test shows different tendency (Fig 26). Deposition and dissolution of Mg need an overpotential during first several cycles. Therefore, the efficiency of Mg/PT cell is around 10% at 1st cycle. However, its efficiency is rapidly increased and then stabilized after 40th cycle with a 90 ~ 95 % capacity (Fig 26b).
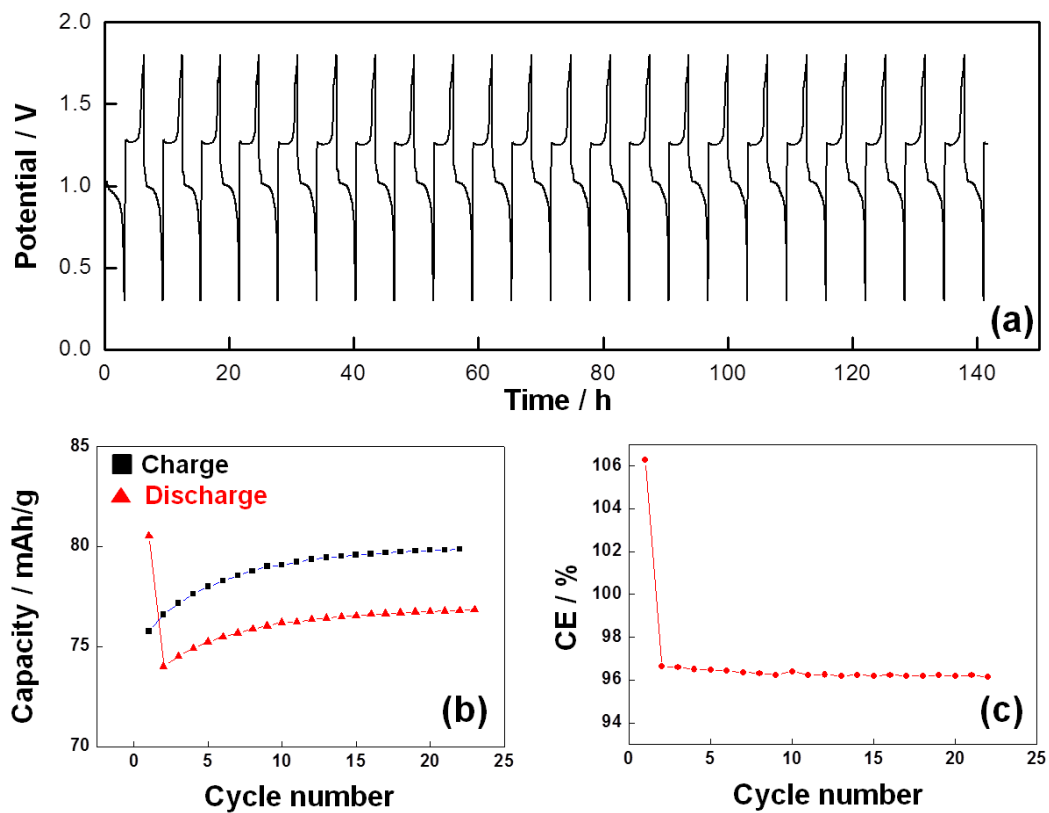
Fig. 25. Coin cell test of the Mg-Mo$_6$S$_8$ system in DPSO$_2$/THF electrolyte containing 0.8M MgCl$_2$ at a constant current rate of 0.2mA (0.2C). (a) charge/discharge profile (b) capacity of vs. cycle number, and (c) columbic efficiency vs. cycle number.
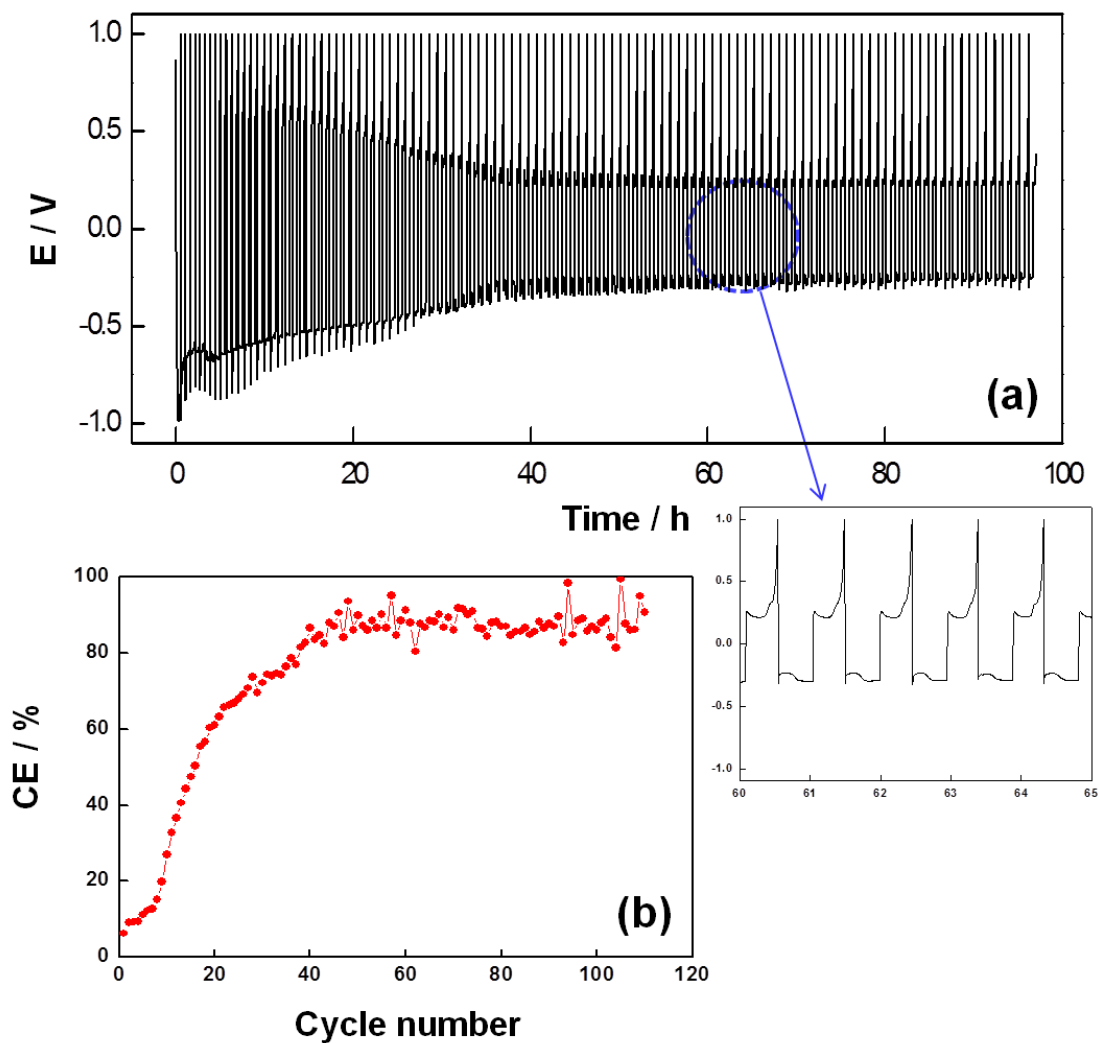
Fig. 26. Coin cell test of the Mg-Pt system in DPSO$_2$/THF electrolyte containing 0.8M MgCl$_2$ at a constant current rate of 0.01mA (a) charge/discharge profile, and (b) columbic efficiency vs. cycle number.

3.2.8 Corrosion of current collectors in DPSO$_2$/THF electrolyte

In the previous study, DPSO$_2$/THF has excellent electrochemical stability within a large electrochemical window and the high Mg deposition/dissolution efficiency. However we could find out columbic effi-

ciency of coin cell test was decreasing slightly in Fig. 25 experiment and anodic charge part of CV in Fig. 24 was increasing after 20cycles. It seems that a corrosion of current collector in chevrel phase was happened in our electrolyte system. Therefore various current collectors were tested for their stability in our system. Fig. 27 shows the CV cycles obtained for Ni, SUS, Al, and Cu in the voltage range of 1 to 3.3 V. CV analysis of these current collectors suggests that it is not stable beyond 2.5 V with the present electrolyte. Nevertheless, Ni electrode exhibits more stable than other ones (Fig. 27). Ni is a suitable candidate as a cathode and anode current collector for magnesium batteries. Further experiment of cathode material on Ni foil for current collector is needed to be carried for next future step. We will handle this issue future study.
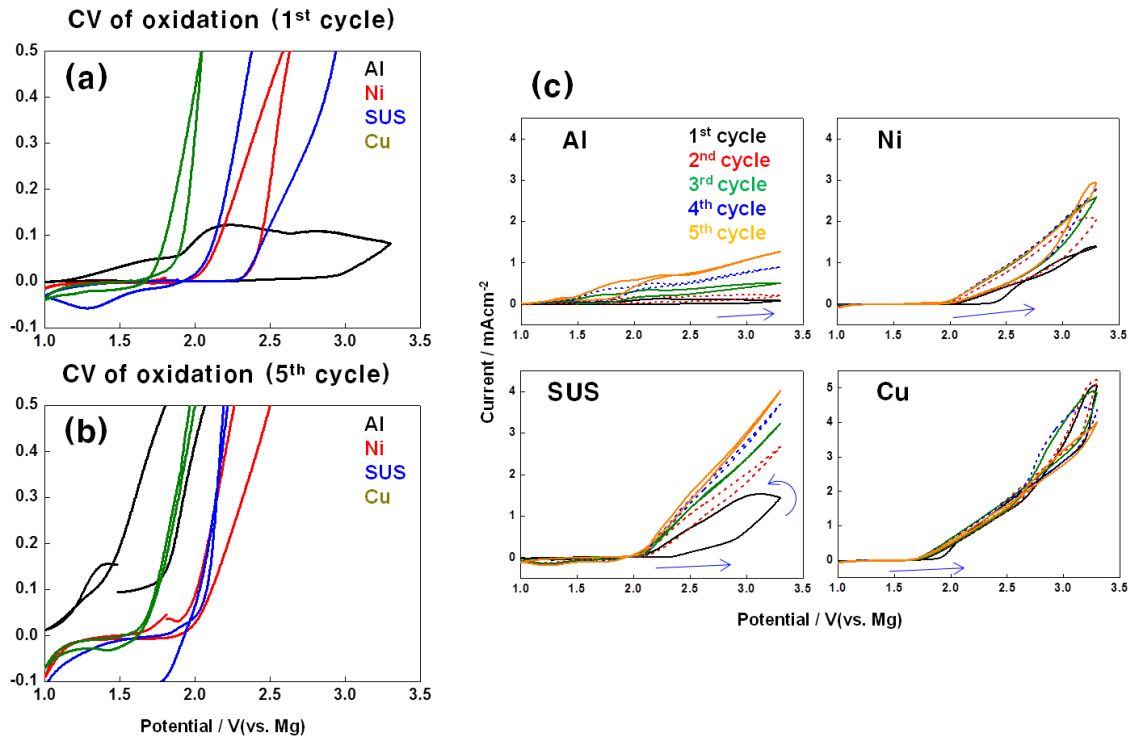
Fig. 27. Oxidation CVs of DPSO$_2$/THF electrolyte containing 0.8M MgCl$_2$ on Aluminum, nickel, SUS, and platinum (a) first cycle, (b) fifth cycle. (c) CVs of Al, Ni, SUS, CU in 5cycle

Ⅳ. CONCLUSION

4.1. Li-ion battery

It was demonstrated that the HF impurity is the key factor to suppress the redox reactions of LIB graphite anodes. The adverse effects of HF were attributed to the HF-induced formation of surface LiF layer, which is more resistive to Li+ transport than organic-rich SEI. More importantly, it was proven that the LiF formation is facilitated at a high V/A ratio. This provides a possible explanation on why graphite composite electrodes for commercial LIBs are less influenced by HF than the HOPG electrodes for model experiments usually performed in the flooded condition. The effect of surface area follows double-layer capacitance values, 333 and 48 $\mu F/cm^2$, emery-PGE and alumina-PGE, respectively.

4.2. Mg-ion battery

We report herein on the development of various electrolytes for Mg rechargeable battery system. Especially, sulfone-based electrolyte solutions which conventional Mg salt ($MgCl_2$) is used are promising candidate for electrolyte of Mg battery. Sulfone-based electrolytes are is able to be cycled Mg deposition-dissolution processes without Grignard reagents. Especially condition of $DPSO_2$ solution adding THF is improved over 80% cycling efficiency in PGE electrode. The conductivity of these solutions is twice more than $DPSO_2$ used alone. Important is their wide electrochemical window, >3 V. In addition, $DPSO_2$/THF electrolyte is able to be used Mg insertion cathode material, Chevrel phases (Mo_6O_8) which is developed of high-energy density, rechargeable Mg batteries. In addition, we found that Ni is an excellent current collector candidate for use as cathode in sulfone/THF electrolyte of Mg batteries.

Sulfone-based electrolytes are still needed to be improved of its cycling efficiency, lower overpotential and ionic conductivity. However, this work provides a stepping stone for extending the applications of reversible Mg electrolyte, without using Grignard reagents.

References

[1] M. Ochida, Y. Domi, T. Doi, S. Tsubouchi, H. Nakagawa, T. Yamanaka, T. Abe, Z. Ogumi, "Influence of Manganese Dissolution on the Degradation of Surface Films on Edge Plane Graphite Negative-Electrodes in Lithium-Ion Batteries" J. Electrochem. Soc. 159 (2012) A961.

[2] Y. Domi, M. Ochida, S. Tsubouchi, H. Nakagawa, T. Yamanaka, T. Domi, T. Abe, Z. Ogumi, "Electrochemical AFM Study of Surface Films Formed on the HOPG Edge Plane in Propylene Carbonate-Based Electrolytes Batteries and Energy Storage" J. Electrochem. Soc. 159 (2012) A1292.

[3] X. Wang, K. Aoki, "Transition of current of lithium intercalation from solution to graphite" J. Electroanal. Chem. 604 (2007) 101.

[4] F.P. Campana, R. Kotz, J. Vetter, P. Novak, H. Siegenthaler, "In situ atomic force microscopy study of dimensional changes during Li^+ ion intercalation/de-intercalation in highly oriented pyrolytic graphite" Electrochem. Comm. 7 (2005) 107.

[5] T. D. Gregory, R. J. Hoffman, R. C. Winterton, "Nonaqueous Electrochemistry of Magnesium" J. Electrochem. Soc., 137 (1990) 775.

[6] Y. N. Nuli, J. Yang, Y. S. Li, J. L. Wang, "Mesoporous magnesium manganese silicate as cathode materials for rechargeable magnesium batteries" Chem. Commun., 46 (2010) 3794.

[7] B. Peng, J. Liang, Z. Tao, J. Chen, "Magnesium nanostructures for energy storage and conversion" J. Mater. Chem., 19 (2009) 2877.

[8] Y. NuLi, Z. Guo, H. Liu, J. Yang, "A new class of cathode materials for rechargeable magnesium batteries: Organosulfur compounds based on sulfur–sulfur bonds" Electrochem. Commun., 9 (2007) 1913.

[9] W. Y. Li, C. S. Li, C. Y. Zhou, H. Ma, J. Chen, "Metallic Magnesium Nano/Mesoscale Structures: Their Shape-Controlled Preparation and Mg/Air Battery Applications" Angew. Chem., Int. Ed., 45 (2006) 6009.

[10] D. Aurbach, Z. Lu, A. Schechter, Y. Gofer, H. Gizbar, R. Turgeman, Y. Cohen, M. Moshkovich, E. Levi, "Prototype systems for rechargeable magnesium batteries" Nature, 407 (2000) 724.

[11] Z. Lu, A. Schechter, M. Moshkovich, D. Aurbach, "On the electrochemical behavior of magnesium electrodes in polar aprotic electrolyte solutions" J. Electroanal. Chem., 466, 203 (1999)

[12] Tuan T. Tran, W. M. Lamanna, M. N. Obrovac, "Evaluation of $Mg[N(SO_2CF_3)_2]_2$/Acetonitrile Electrolyte for Use in Mg-Ion Cells" J. Electrochem. Soc. 159 (2012) A2005.

[13] D. Aurbach, G. S. Suresh, E. Levi, A. Mitelman, O. Mizrahi, O. Chusid, M. Brunelli, "Progress in Rechargeable Magnesium Battery Technology" Adv. Mater., 19 (2007) 4260.

[14] N. Amir, Y. Vestfrid, O. Chusid, Y. Gofer, D. Aurbach, "Progress in nonaqueous magnesium electrochemistry" J. Power Sources, 174 (2007) 1234.

[15] O. Mizrahi, N. Amir, E. Pollak, O. Chusid, V. Marks, H. Gottlieb, L. Larush, E. Zinigrad, D. Aurbach, "Electrolyte Solutions with a Wide Electrochemical Window for Rechargeable Magnesium Batteries" J. Electrochem. Soc., 155(2) (2008) A103.

[16] E. Levi, M. D. Levi, O. Chasid, D. Aurbach, "A review on the problems of the solid state ions diffusion in cathodes for rechargeable Mg batteries" J. Electroceram., 22 (2009) 13.

[17] E. Levi, Y. Gofer, D. Aurbach, "On the Way to Rechargeable Mg Batteries: The Challenge of New Cathode Materials" Chem. Mater., 22 (2010) 860.

[18] S. F. Amalraj, D. Aurbach, "The use of in situ techniques in R&D of Li and Mg rechargeable batteries" J. Solid State Electrochem., 15 (2011) 877.

[19] D. Aurbach, Y. Cohen, M. Moshkovich, "The Study of Reversible Magnesium Deposition by In Situ Scanning Tunneling Microscopy" Electrochem. Solid-State Lett., 4 (2001) A113.

[20] E. Levi, Y. Gofer, Y. Vestfreed, E. Lancry, D. Aurbach, "$Cu_2Mo_6S_8$ Chevrel Phase, A Promising Cathode Material for New Rechargeable Mg Batteries: A Mechanically Induced Chemical Reaction" Chem. Mater., 14 (2002) 2767.

[21] Y. Gofer, O. Chusid, H. Gizbar, Y. Viestfrid, H. E. Gottlieb, V. Marks, D. Aurbach, "Improved Electrolyte Solutions for Rechargeable Magnesium Batteries" Electrochem. Solid-State Lett., 9 (2006) A257.

[22] H. S. Kim, T. S. Arthur, G. D. Allred, J. Zajicek, J. G. Newman, A. E. Rodnyansky, A. G. Oliver, W. C. Boggess, J. Muldoon, "Structure and compatibility of a magnesium electrolyte with a sulphur cathode" Nat. Commun., 2011, DOI: 10.1038/ncomms1435.

[23] C. Liebenow, "Reversibility of electrochemical magnesium deposition from Grignard solutions" J. Appl. Electrochem., 27 (1997) 221.

[24] J. Muldoon, C. B. Bucur, A. G. Oliver, T. Sugimoto, M. Matsui, H. S. Kim, G. D. Allred, J. Zajicek, Y. Kotani, "Electrolyte roadblocks to a magnesium rechargeable battery" Energy Environ. Sci., 5 (2012) 5941.

[25] D. Lv, T. Xu, P. Saha, M. K. Datta, M. L. Gordin, A. Manivannan, P. N. Kumta, D. Wang, "A Scientific Study of Current Collectors for Mg Batteries in $Mg(AlCl_2EtBu)_2$/THF Electrolyte" J. Electrochem. Soc., 160(2) (2013) A351.

[26] M. Tang, K. Miyazaki, T. Abe, J. Newman, "Effect of Graphite Orientation and Lithium Salt on Electronic Passivation of Highly Oriented Pyrolytic Graphite" J. Electrochem. Soc., 159(5) (2012) A634.

[27] M. Tang, K. Miyazaki, T. Abe, J. Newman, "Effect of Graphite Orientation and Lithium Salt on Electronic Passivation of Highly Oriented Pyrolytic Graphite" J. Electrochem. Soc., 159 (2012) A634.

[28] M. Tang, J. Newman, "Why is the Solid-Electrolyte-Interphase Selective? Through-Film Ferrocenium Reduction on Highly Oriented Pyrolytic Graphite" J. Electrochem. Soc., 159 (2012) A1922.

[29] D. Aurbach, Y. Ein-Eli, B. Markovsky, A. Zaban, S. Luski, Y. Carmeli, "The Study of Electrolyte Solutions Based on Ethylene and Diethyl Carbonates for Rechargeable Li Batteries" J. Electrochem. Soc., 142 (1995) 2882.

[30] A. Schechter, D. Aurbach, H. Cohen, "X-ray Photoelectron Spectroscopy Study of Surface Films Formed on Li Electrodes Freshly Prepared in Alkyl Carbonate Solutions" Langmuir 15 (1999) 3334.

[31] V. Eshkenazi, E. Peled, L. Burstein, D. Golodnitsky, "XPS analysis of the SEI formed on carbonaceous materials" Solid State Ionics, 170 (2004) 83.

[32] H. Lee, J.-J. Cho, J. Kim, H.-J Kim, "Comparison of Voltammetric Responses over the Cathodic Region in $LiPF_6$ and LiBETI with and without HF Batteries, Fuel Cells, and Energy Conversion" J. Electrochem. Soc., 152 (2005) A1193.

[33] M. Tang, K. Miyazaki, T. Abe, J. Newman, "Effect of Graphite Orientation and Lithium Salt on Electronic Passivation of Highly Oriented Pyrolytic Graphite" J. Electrochem. Soc., 159(5) (2012) A634.

[34] R. J. Rice and R. L. McCreery, "Quantitative Relationship between Electron Transfer Rate and Surface Microstructure of Laser-Modified Graphite Electrodes" Anal. Chem., 61(15) (1989) 1637.

[35] L. Legrand, M. Heintz, A. Tranchant , R. Messina "Sulfone-Based Electrolytes for Aluminum Electrodeposition" Electrochimica Acta., 40 (1995) 1711.

[36] K. Xu, C. A. Angell, "High Anodic Stability of a New Electrolyte Solvent: Unsymmetric Noncyclic Aliphatic Sultone" J. Electrochem. Soc., 145 (1998) L70.

요 약 문

리튬 및 마그네슘 이차전지용 카본과 마그네슘 음극에서의 전해액 계면 연구

리튬 이온전지의 흑연 음극에서의 충방전 반응이 $LiPF_6$ 전해액에서 발생하는 HF 에 의해 어떻게 영향을 받는지에 대한 연구와 마그네슘 이온전지에서 작동하는 그리냐르계 전해액이 아닌 sulfone 계 전해액을 개발하여 대한 연구이다.

첫 번째로, PGE 전극에서 $LiClO_4$ 전해액 사용 시 리튬이온의 이동특성은 가역적으로 나오지만 LiPF6 전해액 사용시에는 리튬 삽입/탈리 반응이 점차 줄어드는 것을 발견하였다. LiPF6 의 이런 느린 삽입/탈리 반응이 HF 억제제 첨가에서는 향상되었고 반면에 LiClO4 전해액에 HF 첨가에는 오히려 삽입/탈리 반응이 줄어드려 버렸다. 또한 LiPF6 전해액에서 전해액의 양이 줄어들거나, PGE 전극의 표면적이 늘어났을 때 리튬 이온 이동성이 증가하였다. 전해액 양과 전극 표면적 비가 높으면 HF 에 의한 음극 표면의 LiF 생성을 쉽게 만드는 것으로 보여진다. 전해액 양/전해액 표면적 비는 일반 상용 흑연음극에서도 리튬 이온 이동성에 영향을 주었다. 이번 연구를 통해서 오랜 궁금증이었던 'LiPF6 전해액에서 상업적인 리튬전지에선 보이지 않는 리튬 이온 이동성 억제가 실험실의 충분한 전해액 상황에서는 일어나는 이유'에 대해 설명을 해준다.

다음으로, 화학적, 전기화학적 안전성이 취약한 그리냐르계 전해액이 아닌 가역적인 마그네슘 배터리 시스템을 위한 전해액 개발 필요에 대한 연구이다. Sulfone 계 전해액이 여기에서 3 전극 실험을 통해 CV (cyclic voltammogram) 특성이 연구되었다. dipropyl sulfone ($DPSO_2$) 및 ethyl-methyl sulfone ($EMSO_2$) 등의 전해액에 MgCl2 염을 사용하여 특성들이 연구되었다. 특히 DPSO2 전해액에 tetrahydrofuran (THF)을 첨가하였을 때 CV 특성 및 이온전도도가 확연히 증가하는 것을 확인 할 수가 있었다. 그리고 코인셀 실험 결과 이 전해액에서 양극재, Mo_6S_8 과 가역적으로 구동되는 것을 확인하였다. 산화쪽 전압에서 여러 집전체 금속들이 산화하는 모습들을 확인하였는데, Ni 금속을 사용하면 산화전압에 우수한 특성을 보이는 것을 확인하였다.

핵심어: Li-ion batteries, HF, LiF, Mg-ion batteries, Sulfone electrolyte